Aberystwyth University

Monitoring Matang's Mangroves in Peninsular Malaysia through Earth Observations: A Globally Relevant Approach
Lucas, Richard; Otero, Viviana; Van De Kerchove, Ruben; Lagomasino, David; Satyanarayana, Behara; Fatoyinbo, Temilola; Dahdouhguebas, Farid

Monitoring Matang's Mangroves in Peninsular Malaysia through Earth Observations: A Globally Relevant Approach.

Richard Lucas[1,2§], Viviana Otero[3], Ruben Van De Kerchove[4], David Lagomasino[5],

Behara Satyanarayana[3,6], Temilola Fatoyinbo[7] and Farid Dahdouh-Guebas[3,8]

[1]Department of Geography and Earth Sciences, Aberystwyth University, Aberystwyth, Ceredigion, SY232EJ, UK.

[2]School of Biological, Earth and Environmental Sciences (BEES), University of New South Wales (UNSW), Sydney, High Street, Kensington, NSW, 2052, Australia.

[3]Systems Ecology and Resource Management Research Unit, Department of Organism Biology,, Université Libre de Bruxelles (ULB), Av. F.D. Roosevelt 50, CPi 264/1, B-1050, Brussels, Belgium.

[4]Vlaamse Instelling Voor Technologisch Onderzoek (VITO) Research Organisation, Mol, Belgium.

[5]Department of Coastal Studies, East Carolina University, Greenville, North Carolina, USA.

[6]Mangrove Research Unit (MARU), Institute of Oceanography and Environment, Universiti Malaysia Terengganu (UMT), Kuala Nerus, Terengganu, Malaysia.

[7]NASA Goddard Space Flight Center, Biospheric Sciences Laboratory, Greenbelt, Maryland, 20817, USA

[8]Laboratory of Plant Biology and Nature Management, Ecology and Biodiversity, Vrije Universiteit Brussel (VUB), VUB-APNA-WE, Pleinlaan 2, Brussels, Belgium.

[§] Corresponding author at: Department of Geography and Earth Sciences, Aberystwyth University, Aberystwyth, Ceredigion, SY23EJ. Email address: richard.lucas@aber.ac.uk

Abstract

Expansion of rotational timber harvesting of mangroves is set to increase, particularly given greater recognition of their economic, societal and environmental benefits. Generic and standardized procedures for monitoring mangroves are therefore needed to ensure their long-term sustainable utilisation. Focusing on the Matang Mangrove Forest Reserve (MMFR),

Perak State, Peninsular Malaysia, thematic and continuous environmental variables with defined codes or units, including lifeform, forest age (years), canopy cover (%), above ground biomass (Mg ha^{-1}) and relative amounts of woody debris (%), were retrieved from time-series of spaceborne optical and single/dual polarimetric and interferometric radar. These were then combined for multiple points in time to generate land cover and evidence-based change maps according to the Food and Agriculture Organisation (FAO) Land Cover Classification System (LCCS) and using the framework of the Earth Observation Data for Ecosystem Monitoring (EODESM). Change maps were based on a pre-defined taxonomy, with focus on clear cutting and regrowth. Uncertainties surrounding the land cover and change maps were based on those determined for the environmental variables used for their generation and through comparison with independent retrieval from other EO data sources. For the MMFR and also for other mangroves worldwide where harvesting is occurring or being considered, a new approach and opportunity for supporting management of mangroves is presented, which has application for future planning of mangrove resources.

Keywords: Remote sensing, mangroves, classification, monitoring, management.

1. Introduction

Mangrove forests occupy the coastal regions of over 120 countries (Spalding *et al.*, 2010) and these represent a major resource for local and national populations. This was emphasised in the United Nations Ocean Conference in 2017, which highlighted that nearly one billion people are living in coastal communities, many of these are in the tropics and subtropics and in areas supporting mangroves. In these regions, there is considerable interest in increasing the extent and cover of mangrove forests across their potential range whilst ensuring economic returns for

local communities and maximising national and international economic, societal, political and environmental benefits (Bosire *et al.,* 2008, Rönnbäck *et al.*, 2007). Maintaining and restoring mangroves are sensible options that have been increasingly recognised by national governments and the international community, with emphasis placed on ensuring exploitation is sustainable and addresses the well-being of current and future generations (Ellison, 2000, Bosire *et al.*, 2008, Goessens et al. 2014; Huge et al., 2016; Satyanarayana et al., 2017). These options are particularly relevant given the rapid and unprecedented changes in global climate and the need to retain and expand carbon stocks and sinks, address resource demands in coastal regions and particularly where human populations are increasing, and guarantee protection of ecosystem values and services, including those related to biodiversity (Alongi, 2008, Alongi, 2012, Walters *et al.*, 2008, Spalding *et al.*, 2010).

`

Options for generating a sustainable and viable revenue stream from mangroves include rotational timber production, ecotourism (e.g., through conservation) and planned use of resources embedded within or linked to this ecosystem (e.g., invertebrate and fish populations, carbon stocks) (Ellison, 2000, Alongi, 2012, Walton *et al.*, 2006, Lopez-Portillo *et al.*, 2017). Recognising the financial impacts of not maintaining a mangrove cover is also important as these can be substantive and include costs associated with restoring infrastructure and other resources lost following, for example, storms, flooding and sea-level rise (Costanza *et al.,* 1997, Lee *et al.,* 2014, Di Nitto *et al.*, 2014). For this reason, there is a need to better understand the characteristics of their landscape settings, quantify current and past extents, dynamics and values of mangrove forests (with reference to biophysical attributes), be better informed regarding pathways for development and have capacity to predict future resource availability and benefits (Thomas et al., 2017, Lee *et al.*, 2014),

Such efforts have been significantly advanced with the release of up-to-date maps of regional and global mangrove extent (Bunting et al., 2018), height (Fatoyinbo and Simard, 2013), biomass (Simard et al., 2019) and restoration potential (Worthington and Spalding, 2018) as well as mudflat extent (Murray et al., 2019). These baselines provide new opportunities for ongoing monitoring of mangroves and their environs. However, there is a need also to concurrently establish routine, standardized and consistent methods for a) understanding historical, current and future dynamics of mangroves in response to different drivers of change, whether these be natural (e.g., Duke et al., 2017) or anthropogenic (e.g., Thomas et al. 2017, Richards and Friess, 2016) and b) informing communities, landholders and governments of mangrove values and progress toward their sustainable management, restoration, conservation and use (e.g. Huge *et al.*, 2016, Satyanarayana *et al*., 2012, Kairo *et al*., 2001). Considering the additional danger posed by cryptic ecological degradation (Dahdouh-Guebas at al., 2006), Koedam & Dahdouh-Guebas (2008) highlighted the urgent need for creating an early warning system for detecting ecological quality changes and degradation in mangrove forests.

Focusing on the Matang Mangrove Forest Reserve (MMFR) in Perak State, Peninsular Malaysia, this research aimed to establish and demonstrate a globally-applicable, viable and robust framework for monitoring commercially managed mangroves using satellite sensor data. As components, the framework needed to facilitate historical overviews and understanding of the impacts of past and ongoing management, identify changes that were both historical in nature but also as and when new satellite data become available, and inform on potential future changes. To achieve this aim, the methods associated with the Earth Observation Data for Ecosystem Monitoring (EODESM; Lucas and Mitchell, 2017) were used, with this being an

advance on its predecessor, the Earth Observation Data for Habitat Monitoring (EODHaM: Lucas et al., 2014). EODESM generates maps of land cover and change according to the Food and Agriculture Organisation (FAO) Land Cover Classification System (LCCS; Version2), and by integrating environmental variables (EVs) retrieved primarily from Earth observation (EO) data.

The MMFR was selected as the *Rhizophora*-dominated forests have been managed for charcoal and pole production since 1902, making the reserve one of the longest silvicultural management areas globally (Noakes, 1952, Muda & Nik Mustafa, 2003, Chong, 2006). The changes in mangrove cover in the MMFR are rapid because of the nominal 30-year forest rotation cycle and the MMFR was therefore well suited for monitoring using EO (e.g. Aziz et al., 2015, Otero et al., 2019). The clearances and the progression of the logging cycle have also been shown to be readily identifiable within 30 m resolution Landsat and approximately 18 m resolution Japanese L-band Synthetic Aperture Radar (SAR) data and these have proved useful for mapping mangrove extent in the MMFR and for retrieving EVs (Lucas et al., 2020). Otero et al (2019) also determined the advantages of using Landsat sensor data and derived indices for ageing forests and understanding dynamics associated with the management process. Otero et al. (2018) and Lucas et al. (2020) further identified the role that unmanned airborne vehicles (UAVs) can play in providing more detailed and supportive information on several EVs (e.g., canopy height). Whilst this study served primarily to support ongoing management of forests in the MMFR by the Malaysian Forestry Department, the approach was developed such that it was relevant and applicable to other areas where future harvesting is taking place or is proposed (e.g., in Malaysia and Indonesia, including West Papua and the Arafura Sea mangrove area; Chong, 2006, Sillanpäa *et al*., 2017).

2. Study area

The MMFR (Figure 1) is located on the western coast of Peninsular Malaysia within the tropical monsoonal region (Köppen climate classification category of Am; mean monthly temperatures exceeding 18° in every month and a dry season) and occupies an area of approximately 40,000 ha (Ariffin and Mustafa, 2013). The area receives an annual rainfall ranging from 2000-2800 mm and average air temperatures ranges from 22-33° C (Ariffin and Mustafa, 2013). Being protected from ocean waves and tidal influences (spring tide amplitude of 3.3 m) (Asthon et al., 1999), the MMFR has extensive mangrove forests that colonise and thrive along the coastline of ca. 51.5 km (Goessens et al., 2014).

The management divides the area of the MMFR into four zones: protective, productive, restrictive productive and unproductive (Ariffin and Mustafa, 2013). The productive and restrictive productive zones are managed under a 30-year rotation cycle and are the areas where timber extraction takes place. These zones are mainly composed of *Rhizophora apiculata* Blume and *R. mucronata* Lamk. (Ariffin and Mustafa, 2013). Within the productive and restrictive productive forests, the logging cycle involves clear-felling of the coupes. Areas between 2.2 ha and 6.6. ha are assigned by the local management to different charcoal contractors that perform the clear-felling operations (Ariffin and Mustafa, 2013) over the course of approximately 24 months (Lucas et al., 2020). The timber is removed but the remnants of the cut stumps, primarily the prop roots of the dominant *R. apiculata* and *R. mucronata*, and woody debris (branches and some trunks) remain. After cutting, subsequent forest growth in coupes takes place through natural regeneration assisted by planting if needed, with the extent and production assessed after 2 years of growth. After approximately 15 and 20 years of growth,

the forests are typically thinned (Ariffin and Mustaffa, 2013) and eventually recleared once the forests have reached maximum productivity (i.e., at approximately 30 years). The Forestry Department has favoured the establishment of the two *Rhizophora* species previously mentioned, with these being pest-resistant and highly calorific. This has resulted in relatively even-aged monocultures. However, within the MMFR, 25 other mangrove species occur although these are largely confined to the protective zones (Ariffin and Mustafa, 2013).

3. Methods

3.1 Available data

For the present study, all available Landsat Thematic Mapper (TM) and Enhanced TM (ETM+) surface reflectance data (%) over the period 1988 to 2016 were obtained from the United States Geological Survey (USGS; Landsat World Reference System Path 128, Row 57). The nominal spatial resolution is 30 m. Cloud free Landsat scenes for individual dates were available for most years, with the exception of 2012 because of failure in the Landsat-7 ETM+ Scan Line Corrector. However, where cloud cover occurred in all images acquired in a particular year, composites were necessarily generated. This was achieved by first selecting the image in each year with the least amount of cloud and cloud shadow and then replacing affected pixels with those that were cloud-free in other images from the same year (Otero et al., 2019). On average, only 3 % of pixels needed to be replaced within the images with the least cloud cover. The use of composites was considered acceptable given that clear felling of coupes takes place over several years and because of the evergreen nature of mangroves in the MMFR. It should be noted, however, that a seasonal response has been observed in mangroves in other regions (Pastor-Guzman et al., 2018).

All available Japanese Earth Resources Satellite (JERS-1) SAR, Advanced Land Observing Satellite (ALOS) Phased Arrayed L-band SAR (PALSAR) and ALOS-2 PALSAR-2 data (nominally 18 m spatial resolution) were obtained through the Japanese Space Exploration Agency (JAXA) Kyoto and Carbon (K&C) Initiative. The JERS-1 SAR provided L-band horizontally (H) polarised transmitted and received (L_{HH}) data whilst the ALOS PALSAR series acquired data at both HH and vertically (V) received (HV) polarisations (L_{HV}). JERS-1 SAR data were obtained for the periods 12th March 1993 to 26th August 1997 (L_{HH} only; 20 scenes), ALOS PALSAR Fine Beam Single (FBS; L_{HH}) and Fine Beam Dual (FBD; L_{HH} and L_{HV}) for 1st June 2006 to 23rd January 2011 (45 scenes), and ALOS-2 PALSAR-2 FBS and FBD for 2nd October 2014 to 29 September 2016 (8 scenes). These corresponded to the periods when the sensors were in operation. Observations were not available from 1997 to early 2006 (a period of approximately 9 years) and late 2011 to 2014 (approximately 3.5 years). Scenes with both full and partial coverage of the MMFR were used. Three scenes were excluded as they encompassed only a very small part of the MMFR. All SAR data were calibrated to the backscattering coefficient (σ^o, dB – Table 1; Lucas *et al.*, 2020). The final dataset (98 scenes; Figure 2) therefore consisted of annual Landsat sensor (29th July 1988 to 18th March 2016; 28 single or composite scenes) and all available Japanese L-band SAR data (70). NASA Shuttle Radar Topographic Mission (SRTM) data (30 m spatial resolution) were acquired between 11th and 22nd February 2000. Tandem-X data (2011-2015; 12.5 m spatial resolution) were also obtained for the MMFR and the surrounding landscapes. All datasets were finally resampled, using gdal, to 12.5 m spatial resolution following pre-processing and calibration so as to align with that of the TanDEM-X (Lucas et al., 2020).

In July 2016, and as described by Otero et al. (2018) and Lucas et al. (2020), DJI Phantom 3 true colour (RGB) Unmanned Airborne Vehicle (UAV) imagery were obtained over nine 1 ha plots in the MMFR, from which < 1 m spatial resolution orthomosaics and canopy height models (CHMs) were generated.

3.2 Land Cover Classifications

Based on the concepts of EODESM, land cover classes according to the FAO LCCS taxonomy (Figure 3) were generated for all 98 observation dates from environmental variables (EVs) retrieved from combinations of Landsat sensor, L-band SAR and interferometric SAR, with these relating primarily to vegetation. All processing was undertaken using python scripts and the RSGISLib software of Bunting et al. (2013). This included pixel-level segmentation of the MMFR area to a spatial resolution of 12.5 m, attribution of segments with EV data using Raster Attribute Tables (RAT) stored through the KEA image format (Clewley et al., 2014, Gillingham and Bunting, 2014), and the combining of EVs to form land cover classes defined by the FAO LCCS taxonomy. All EVs used for the classifications were retrieved using relationships established with the resampled data. A flow chart outlining the overall approach is given in Figure 4 and further details in EODESM can be found in Lucas and Mitchell (2017), Lucas et al. (2019) and other forthcoming publications.

3.2.1. Classification to FAO LCCS Level 3

The generation of FAO LCCS Level 3 maps through EODESM required separate classification of five land cover types – vegetation, aquatic, cultivated/managed and artificial urban and artificial water – with these assigned a value of 1. The inverse classes of non-vegetated, terrestrial, semi-natural/natural, naturally bare surfaces or water were assigned a value of 0.

The LCCS Level 3 classification was then generated through cross tabulation of these binary layers (Lucas and Mitchell, 2017).

For each of the 98 dates of observation, vegetated areas were identified as having a Landsat-derived Normalised Difference Moisture Index (NDMI) > 0.37 (range 0.32 to 0.39) or $L_{HH}\sigma^o <$ -8.0 dB (range -7.2 to -9.0 dB). These thresholds were determined for each date through visual interpretation of each Landsat or L-band SAR image and by referencing scenes acquired on the dates prior to and following. Variability in the thresholds was low and was attributed to prevailing conditions at the time of the satellite observations, including tidal inundation and precipitation that influenced the moisture contents of the vegetation and ground surface. Together with open water, all remaining areas of the MMFR land area were assigned to a non-vegetated category, with the majority occurring because of logging activities. These areas exhibited a lower NDMI, because of the lack of a vegetation (canopy) cover following clearing. The high $L_{HH}\sigma^o$ observed in these areas was attributed to enhanced scattering of microwaves from cut stumps and woody debris remaining on the ground surface (Lucas et al., 2020). The aquatic class (summarised for each year) encompassed areas of mangrove within the MMFR and all water bodies. Urban areas, which consisted primarily of the town of Kuala Sepetang but encompassed other small settlements, were associated with pixels in the 2016 Landsat image with an NDMI < 0 (Otero et al., 2019). This threshold was determined through reference to Open Street Map (OMS) data for the region. The urban extent was assumed to be constant for each preceding date in the time series, which was justified as changes in area had minimal impact on the extent of mangrove forest. All cultivated areas were outside of the MMFR and so this class was excluded from the classification, and all water areas were considered to be natural. Following generation of the 5 layers representing the extent of vegetation, aquatic, cultivated/managed and artificial urban and artificial water and their opposites, LCCS

classifications to Level 3 were produced from their combination for each of the 98 observation dates over the period 1987-2016.

3.4 Classification based on LCCS Level 4

Within each LCCS Level 3 class, further descriptions were provided by considering what is termed here the Level 4 taxonomy, with particular focus on the primarily vegetated natural/semi-natural and non-vegetated aquatic categories (see Figure 3). In this case, more specific EVs were used to create raster layers whose values corresponded to pre-defined string codes in the LCCS taxonomy (e.g., A4 for trees, B5 for > 14 m, or A1 for water in the lifeform, canopy height and water state modules respectively). These were then combined to generate codes and descriptive labels for the different land cover categories. Within this modular hierarchical phase, mangroves were described on the basis of their canopy cover and height (from which physiognomic lifeform was described), leaf type and phenology. As an example, and of relevance to mangroves, the class A24.A3.A21.B5.C1.D1.E1, which is formed from the combinations of codes and written out in the RAT, describes "aquatic (A24) trees (A3) that have an open to closed (40-100 %) canopy (A21), are tall (>14 m; B5) continuous (C1) broadleaved (D1) and phenologically evergreen (E1)". Additional attributes would be "on flooded land (tidal), dominated by *Rhizophora apiculata* with an AGB (Mg ha^{-1}) of 123 Mg ha^{-1}". Non-vegetated classes included water (described on the basis of liquid state) and bare areas (unconsolidated material; primarily mud). A summary of the target EVs and their generation from EO data is provided in the following sections.

3.4.1. Canopy cover (%)

Tree canopy cover represents the proportional, vertically projected area of vegetation (including leaves, stems, branches, etc.) above a given height. For this study, estimates of canopy cover were obtained on a near annual basis from 1988 to 2016 from the Landsat sensor data. Otero et al (2019) indicated that the Landsat-derived NDMI was sensitive to canopy cover and also better suited than the Normalized Difference Vegetation Index (NDVI) because of its greater dynamic range (approximately 0.65 compared to 0.28 for the NDVI). On this basis, Lucas et al. (2020) established a relationship between the NDMI and canopy cover (%), as determined from the Phantom-3 DJI RGB imagery, which was used to estimate canopy cover for each year from the single date or composite Landsat data (Figure 5a).

3.4.2. Canopy height (m)

Based on acquisitions of DLR's interferometric Tandem-X (TDX) over the period 2011 to 2015, a CHM was generated for the MMFR mangroves (TDX$_{CHM}$; Lucas et al., 2020), with this corresponding through visual comparison to the Landsat NDMI image of 15th June 2015. The assumptions were made that the mean elevation of the underlying topography in the intertidal area was 0 m (mean sea level) and the slope was 0° (i.e., flat). The processing of the TanDEM-X Digital Surface Model (DEM) data to a ground resolution of 12.5 x 12.5 m was undertaken using the methods outlined in Wessel (2018) and is described in Lucas et al. (2020). The TDX$_{CHM}$ was validated against eight CHMs retrieved from the Phantom DJI visible imagery acquired in 2016 (RMSE 1.94, R^2=0.89), which gave confidence in its use for quantifying canopy height across the MMFR. A CHM was also generated from the 2000 SRTM data (SRTM$_{CHM}$) using the approach of Simard et al. (2018) (Lucas et al. 2020).

3.4.3. Vegetation lifeform, leaf type, phenology and stratification

The FAO LCCS differentiates lifeforms according to woody (trees and shrubs) and herbaceous (graminoids, forbs). Woody plants that are > 5 m are classified as trees. However, if the plant has a physiognomic aspect of a tree, then this threshold is lowered to > 3 m (Di Gregorio, 2016) Mangrove lifeforms (trees) were defined on the basis of the height of the upper canopy and differentiated using thresholds of > 3 - < 5 m and >= 5 m respectively so as to indicate early regrowth (Figure 5b). The former height range is generally associated with woody shrubs rather than trees, but woody plants with a physiognomic aspect of trees are classified as such if > 3 m and < 5 m in height. Herbaceous vegetation was considered to be largely absent from the MMFR or occupying land parcels that were smaller in area than the 30 m pixel resolution of the Landsat sensor data. The leaf type and phenology descriptions were defined from knowledge, as all mangrove forests in the region are broadleaved and evergreen. Palms (mostly pinnate leaf type) and pine plantations (needle-leaved) were confined primarily to the terrestrial landscapes and were not included in the classification. Information on canopy layering was absent but managed forests were assumed to have one primary layer. The primary (virgin) forests are structurally diverse, as evidenced by the wider range of diameter densities reported by Otero *et al*. (2018), and hence can be considered as having at least two layers. However, quantitative measures of the height and cover of layers below the upper canopy (which can be described within the LCCS) were not available.

3.4.4. Above ground biomass (Mg ha^{-1})

Although not used directly in the FAO LCCS, the above ground biomass (AGB, Mg ha^{-1}) of mangroves within the MMFR, and based on the observation date of 15th June 2015, was estimated from the TDX$_{CHM}$. This was achieved by using a power relationship established by

Fatoyinbo et al. (2017), which utilised data from 51 field plots inventoried in the Zambezi Delta in Mozambique. The AGB for these plots was estimated using the allometric equations of Komiyama et al. (2008), which included measurements obtained originally from harvesting in the MMFR and tree diameter (D_{130}) as the dependent variable.

3.4.4 Descriptors of non-vegetated land covers

All areas of estuarine and oceanic water were coded based on knowledge and according to their state (liquid), flow (moving), sediment loads (turbid in the near shore environments) and inundation status (tidal), as dictated by the FAO LCCS taxonomy. Unconsolidated (fine grained) material was assumed on the exposed mudflats.

3.5. Time extrapolation of biophysical variables.

For each of the 98 dates of observation, the extent of clearance was associated with areas mapped as unvegetated in the LCCS Level 3 classification. By comparing maps of forest clearings generated using the thresholds of Landsat NDMI or $L_{HH}\sigma^o$ between 29th July 1988 (the first Landsat observation) and 29th September 2016 (the last ALOS-2 PALSAR-2 observation), time (in days) since clearing was estimated. The maximum age was 10,289 days (or 28.3 years) on the 29th September 2016. An estimate of the time since clearing (in days) was then generated for each of the remaining 97 dates (Lucas et al, 2020), with only areas cleared since 29th July 1988 being considered. Significant changes were only observed on 68 dates, with this attributed in part to images acquisitions on proximal dates. The time in days was converted to forest age in years and months for ease of interpretation. Natural regeneration and/or direct planting (where necessary) was considered to occur from the date when the clearing was first detected.

Other areas in the productive zone of the MMFR were also at different stages of growth on the 29th July 1988 but were not able to be mapped because of similarities with mature forest in both the NDMI or $L_{HH}\sigma^o$ However, by assuming that all forests observed as being cleared were 30 years old at the time of clearance, their age was able to be estimated back in time and for one rotational cycle (to 1958). Whilst not directly used in this study, these estimates of forest age prior to each clearing event were included in the mapping so as to place the actual observed changes in the context of the previous logging and regrowth cycles.

Once established, the estimates of forest age provided a mechanism for estimating other EVs for each observation date. Estimates of canopy height were extrapolated to all 98 dates of observation using a non-linear relationship established between forest age (in 2015) and the TDX_{CHM} (Table 1 – Equation 1; Figure 6a). These data were also used to generate a lifeform layer for each date that discriminated forest stands that were between > 3 and < 5 m (early stages of regeneration) and >= 5 m. The estimates of AGB derived from the TDX_{CHM} were used to establish a relationship with the age of forests on September 29th 2016 (Table 1 – Equation 2; Figure 6b), which was then used to estimate the AGB for each of the 98 dates of observation and back to July 1988. Landsat sensor data were only available on an annual basis, either as single-date images or composites from multiple dates within the year. Hence, the canopy cover was assumed to remain constant within any one year unless a clearing event had occurred. On this basis, estimates of relative canopy cover (%) were generated for each year based on the Landsat-derived NDMI.

For each date of SAR observation only, and based on the clearing date, relative amounts of non-photosynthetic vegetation (NPV) in the form of woody debris (cut stumps and roots and branches: %) were inferred from the linear decline in the L_{HH} Digital Number (DN) from a maximum (approximately 7000 DN or -6.1 dB) following clearing to a minimum (approximately 3000 DN or - 13.5 dB; Lucas et al., 2020). This decline takes place over a period of approximately 8 years but is reversed beyond this time because the wood debris has largely decomposed, and live trees regenerating or planted within the stand attain a size (and AGB) that is collectively sufficient to evoke double-bounce and subsequently volume scattering (Lucas al., 2014; 2020; Table 1– Equation 3; Figure 6c). This transitional phase can be further described as the continued decline in L-band scattering beyond 5-6 years since clearing (associated with decomposition of larger woody elements) is mirrored by an increase in the NDMI. The cross over between these two measures indicates when the wood debris is overtopped by the increasing amount of foliage in the canopy (Otero et al., 2019; Lucas et al., 2020). However, this debris is still detected at L-band HH in particular because of penetration of microwaves through the foliage and smaller branches of this canopy. Hence, the trends in L_{HH} and NDMI provide a unique insight into the nature and timing of the processes of decomposition and regeneration occurring in the first decade following clearing.

Using the framework of the Level 3 classifications for each observation date, more detailed descriptions to Level 4 were generated using EVs associated primarily with the vegetation and water categories listed within the FAO LCCS taxonomy but also those that were external (namely AGB and NPV). The resulting map legends together with the component and cumulated codes and their translation to descriptive text were stored within the RAT for each date.

3.6. Classifications of land cover change (1988 to 2016).

By comparing a) the LCCS Level 3 categories, b) LCCS Level 4 component codes (e.g., B6 to B5; 3-7 m to 7-12 m in height) and, c) EVs external to the taxonomy (e.g., AGB, NPV) between any two time-separated periods (available for each observation date) and referring also to the pre-change and post-change states and conditions, evidence-based change maps were generated. This approach, described by Lucas and Mitchell (2017), defines change categories *a priori* and identifies and selects layers that might provide evidence for these changes. Descriptions of these changes are then based on the cumulation of this information. The main target categories demonstrated in this study were clearing (i.e., logging) and regrowth.

4. Results

4.1 Temporal estimation of EVs

The comparison of maps of forest age over the 28-year period (since July 1988 and two years short of a full 30-year rotation) highlighted the progressive logging of forests as they matured and subsequent ageing of naturally regenerating and/or planted forests within each coupe. Examples of these are given in Figure 7a, whereby the increasing age of forests following clearing events is tracked. Subsets of height and AGB estimates for these same dates, and estimated from age, are given in Figure 7b and c respectively and convey the vertical development of the canopy and accumulation of above ground carbon by the forests over time. Temporal information on changes in tree growth stage (lifeform) was also generated from the height information and the decomposition of woody material was inferred from the L-band SAR data. Prior to the dates when clearances were detected, the age of forests was backdated for each time-step by assuming that these had been cleared when they had reached 30 years of

age. Within the 318.1 km^2 for which the age of forests was estimated from the time-series of satellite sensor data and for the productive zone, 258 km^2 was cleared from 29th July and on the 29th September 2016 (Figure 8). The rates of clearing between dates varied over the time-series but was generally averaged about 3.79 km^2 (range 0.28 – 14.1 km^2). Rates of clearing were comparatively high from 2014 onwards. The greater frequency of observations during the acquisitions of L-band SAR data provided more information on the clearing rates and patterns.

4.2 Land Cover classifications from variables

Land cover classifications were generated for the MMFR for each of the 98 observation dates and according to the FAO LCCS Level 4 taxonomy. Examples are illustrated in Figure 8 (for 30th July 2000 and 29th September 2016), with each constructed from a range of EVs used directly within the LCCS taxonomy. Each land cover description was augmented with additional information external to the FAO LCCS taxonomy (e.g., AGB, woody debris and also age). As EVs are consistently retrieved for each date, comparisons can be undertaken for any two time-separated points and used to highlight changes that have occurred historically.

The LCCS legend for each pixel was stored within the KEA RAT, with this allowing export to shapefiles for any year through python scripts. This collation of different EVs derived from satellite sensors observing in different modes (e.g. optical, single and dual polarisation and interferometric SAR) provided a mechanism by which to collectively describe and summarise the structural composition and complexity of the mangrove forests as well as the characteristics of the non-forested areas, including recent clearances.

The accuracy of the classification is dependent upon that of the EV layers used as input, with these indicated in Lucas et al. (2020) and Table 1. However, a further indication of accuracy was obtained by comparing the estimates of canopy height for 2000 obtained a) by applying the relationship established between the TDX_{CHM} and forest age (for 2015) to the age class map for 2000vand b) from the $SRTM_{CHM}$ (Figure 10). The map comparison indicated a close correspondence in both the distribution of logged coupes, noting that the SRTM data were not used for the generation of the forest age maps, and also in the spatial distribution of forests within different height ranges. The close correspondence was also confirmed by comparing estimates extracted from 438 polygons of between 1 ha and 1 km^2 in area and located over relatively homogeneous forests of varying age (RMSE = 5.28 m). Greater homogeneity in the distribution of height retrieved from the age class map was observed when compared to the more direct measures from the SRTM, with this resulting from the formation of segments of similar age within the time-series of Landsat and L-band SAR data.

4.3. Changes in LCCS categories and EVs.

Changes between major land cover were first identified by comparing the Level 3 classes between two periods, and where these differed, major transitions in the extent of broad land covers were indicated. An example (Figure 11a) is the change from aquatic natural/semi-natural vegetation (comprised of mangroves) to naturally bare surfaces and *vice versa*. In these cases, information on the states of both categories prior to and following changes can be obtained through reference to the Level 4 categories and EVs external to the LCCS. Where the Level 3 classes remained the same, however, the FAO LCCS component codes at Level 4 (e.g., relating to canopy cover and height) and EVs external to the LCCS (e.g., AGB) provided

information on changes in condition (Figure 11b). Note that both canopy height and AGB were derived from forest age. This information was then collectively cumulated between the two time periods to allow mapping and more comprehensive descriptions of the two pre-defined change categories of clear cutting (logging) and regrowth (Figure 11c). Logging, as an example, was linked to a Level 3 change from natural/semi-natural aquatic vegetation (mangrove) to a bare surface but also a total loss of canopy cover and height. Regrowth was conversely identified initially as a transition from a naturally bare surface to natural/semi-natural aquatic vegetation. This was linked to the removal and decomposition of woody debris, which was evidenced by a progressive reduction in $L_{HH}\sigma^o$ followed by progressive increases in canopy cover, and obscuration of the forest floor and remaining debris, as well as height and AGB and transitions between lifeform classes (trees >3-5 to 5 m to > 5 m). Thinning of the productive forests typically occurs at 15 and 20 years, but this was unable to be reliably detected from the available remote sensing data. The changes identified were again stored internally within the RAT as were transitions within EVs (e.g., age, AGB and woody debris).

5. Discussion

5.1. Use of EVs for land cover classification.

Exploiting EVs to generate land cover and change classifications based on the FAO LCCS taxonomy and within the framework of EODESM provides a robust, reproducible, flexible and understandable approach to establishing the status and monitoring mangroves in the MMFR. The nominal 30-year rotation logging cycle and rapid growth rates of mangroves provided a dynamic landscape in which to evaluate this approach. Of note is that retrievals and associated classifications can be undertaken at any spatial scale and for different points in time provided relevant data are available.

This study has specifically demonstrated how optical, L-band SAR and interferometric SAR can be used for EV retrieval. However, EODESM allows integration of a wide range of EVs for classification and description and these can be retrieved from any sensor operating in appropriate and relevant modes and for which algorithms exist for retrieval or can be developed. This is because the classifications of land cover and change and associated descriptions are based on the integration of EVs with defined codes or units. As such, the approach is applicable to landscapes globally. The retrieval of EVs and associated classifications of land cover and change is also scale independent. As an example, classifications can be generated from very high (< 2 m) imagery, such as the Worldview-2 optical sensor and airborne (including drone) datasets. The use of Worldview-2 is advantageous as it offers stereo capability and potential to retrieve canopy height (Lucas et al., 2020). These data can also provide more detailed information on tree and forest dynamics, including dominant tree species compositions, although their current cost may be prohibitive. Land covers and change in the landscape proximal to the MMFR were not mapped as EVs were unable to be reliably retrieved, primarily because of the lack of supportive ground data. However, EODESM is considered to be particularly suitable for application to other land covers and also mangrove areas that might be subject to management in future years.

Estimation of forest age was an essential component of the temporal classifications as other attributes (e.g., canopy height, AGB and lifeform) depended on relationships with this variable. With a nominal 30-year rotation cycle, the estimation of age requires the use of Landsat sensor data as these have been acquired since the mid-1980s. Annual observations are generally sufficient for mapping given that clearances remain evident within both Landsat and L-band

SAR data for up to 8 years after the clearing event and regrowth following natural colonisation or replanting is progressive as forests mature. However, the integration of L-band SAR or higher frequency optical (including Sentinel-2) data for selected periods provides an opportunity to obtain more detailed information on the location and timing of logging and insight into the formation of logging coupes (Lucas et al., 2020). L-band SAR data are particularly useful given capacity for data acquisitions regardless of weather and illumination conditions and a recommendation is that such observations be used to capture sub-annual observations of change, with a six-month repeat considered sufficient. In the future, L-band sensors such as the ALOS-4 PALSAR-4 and NISAR will provide new datasets that will support ongoing monitoring of mangroves in the MMFR and hence early adoption of these data would be beneficial. These data provide greater capacity for mapping clearances compared to C-band SAR, which provide less discrimination between vegetated and unvegetated areas and lifeforms.

Canopy height was able to be retrieved from the TanDEM-X interferometric SAR data and AGB could be inferred from these data. The use of age information to infer structural attributes (namely canopy height and AGB) over extended periods was essential given the restricted acquisition times of interferometric SAR data. This is also unavoidable given that some variables (e.g., canopy height) are not able to be retrieved on a frequent basis because of the lack of satellite sensors operating in specific modes (in this case, interferometric SAR). However, the close correspondence with the height retrieved from the SRTM indicated that the use of age information provided a viable approach for retrieving the height of mangroves that are under rotational management. Natural variations in height and AGB may nevertheless occur because of adverse or favourable growth conditions, such as prolonged inundation or

changes in nutrient input, which can lead to errors in when these EVs are estimated from age alone. This was highlighted in the comparative study of Otero et al. (2019), which indicated differential recovery in different forest stands as a function of location (e.g., distance to water). Other sources of height information could also be integrated to inform on the dynamics of mangroves and to validate height or AGB maps derived from age. These include data from the ICESAT-2 and the Global Ecosystem Dynamics Investigation (GEDI; both launched in 2018), which could be exploited in future years. For canopy cover, and as with many EVs requiring optical data for retrieval, sub-annual estimates were difficult to obtain from the Landsat NDMI because of cloud cover in many scenes and hence the classification within years needed to refer to the single date or annual cloud-free composites.

Many studies have advocated the use of L-band SAR backscatter, and particularly $L_{HV}\sigma^o$, for retrieving the AGB of woody vegetation because of the asymptotic increase with AGB up to approximately 60-100 Mg ha^{-1} (e.g., Luckman et al., 1998; Hamdan et al., 2014). However, within the MMFR, both $L_{HH}\sigma^o$ and $L_{HV}\sigma^o$ fluctuated over the 30-year rotational cycle (Lucas et al., 2020), which compromised retrieval of AGB from these data. A further limitation of using Japanese L-band data is that the archive omits the periods pre-1992, 1999-2006 and 2011-2014, which prevents estimation of AGB but also the retrieval of relative amounts of woody debris from SAR outside of these period. The Landsat sensors have been acquiring data every 16 days since the mid 1980s to the present day and can therefore be used to fill gaps in the L-band SAR temporal coverage and allow better estimation of forest age. Woody debris is less able to be detected from Landsat sensor data and hence such information cannot be obtained without the use of L-band SAR.

The FAO LCCS does not consider plant species but the EODESM system allows for such information to be included as an additional descriptor of the land cover classes. However, mangrove species were difficult to discriminate from the Landsat sensor data, largely because differences in structural development led to a high level of variability in near infrared (NIR) and shortwave infrared (SWIR) reflectance within and between forests with different species dominance and over time. The majority of mangroves in the productive zone were dominated by *R. apiculata* and *R. mucronate* with other species being less prevalent. The exception was along the coastal margins, where historically (and also today) mangroves have been dominated by *Avicennia-Sonneratia* species (Ariffin and Mustafa, 2013). Whilst some spectral differences in forests dominated by these different species were evident, particularly within the red edge and NIR Worldview-2 data, these were insufficient to allow discrimination from the Landsat sensor data (which lacks a red edge channel). However, it was noted that early regrowth forests of lower stature and dominated by *Rhizophora* species identified in the DJI Phantom RGB imagery were spectrally similar in the Worldview-2 red edge and NIR data to taller (e.g., > 10 m) *Bruguiera* species, but became more distinguishable over time. Hence, the combination of reflectance and canopy height data might provide a future avenue for discrimination of several dominant species in the MMFR. Further information on non-vegetated land covers (e.g., water, bare surfaces) can be included within the LCCS classification (e.g., tidal extent, water flows and sediment loads), but spatial datasets representing these were not available for this study and were necessarily based on knowledge.

5.2. Detecting change

The integration of the component land cover classes and EVs for generating evidence-based change mapping represents a powerful approach to full quantifying and understanding the

cycles of management within the MMFR. Four broad stages within the rotation can be described both from the ground and from remote sensing data (Figure 12). Whilst several of the EVs can be retrieved or estimated directly from the satellite sensor data (e.g., canopy cover, height, AGB, relative amounts of woody debris), knowledge can also be incorporated into EODESM. For example, mangroves are broadleaved (Goessens et al., 2014, Otero et al., 2018), typically evergreen (with some exceptions; Pastor-Guzman et al., 2018) and tidally inundated. Many of the changes occur concurrently, including the decomposition of woody material and the progressive structural development of forests and accumulation of AGB, which facilitates mapping of several change events or processes.

Evidence of clearing, which can take place over a period of up to 2 years for each coupe, includes a sudden loss of canopy cover (%) and forest height (m) as trees are felled and the wood debris (non-photosynthetic material (%) remaining as cut stumps and discarded branches) leads initially to a rapid increase in L-band backscatter, particularly at HH polarisations. As the wood debris decomposes or is removed through tidal movement of water, the $L_{HH}\sigma^o$ also progressively decreases to a minimum, with this assumed to be linear. The NDMI conversely reflects the increase in canopy cover which reaches full (approximately 100%) vegetation cover after about 5.9 years on average (Otero et al., 2019). However, the high $L_{HH}\sigma^o$ indicates that woody debris is still present, although it is shielded from view by the closed canopy cover. Once a full canopy is established, an increase in both $L_{HH}\sigma^o$ and $L_{HV}\sigma^o$ is observed as the individual trees increase in size (diameter and height) and transition from trees (3-5 m) to trees ($\geq$ 5 m in height), with this reflecting the progressive accumulation of biomass (Mg ha^{-1}) within the wood associated with an increase in canopy cover and height. Thinning of the forests is best indicated by a decrease in canopy cover at approximately 20 years, although this is difficult

to discern from optical or SAR data. The forests attain their maximum height and cover at about 30 years of age, after which felling again takes place and the cycle is repeated.

To better identify the two time steps between which comparisons in LCCS codes and EVs are most useful, change detection algorithms can be used with candidates being cross correlation analysis (Tarantino et al., 2016) and the Breaks For Additive Season and Trend (BFAST; Verbesselt et al., 2010). For the MMFR, such methods could be adopted to routinely detect the timings of clear cutting and hence when to also target EO data for describing the pre and post clearing conditions within the 30-year growth cycle. The time since clearing, and hence the age of forests, can also be quantified with each new image acquisition. Similarly, these data can be used to track the progression of forest structural development and AGB accumulation and turnover. Time-series comparison of descriptions from the two identified time stamps discern the nature of change events or processes (e.g., deforestation, decomposition of woody debris, attainment of full canopy cover, growth and thinning) based on evidence, which is a common requirement for management. Classifications are able to be easily updated as and when new imagery are acquired and using EVs retrieved directly or inferred from the relationships with forest age. Furthermore, as knowledge of the age of forests is known, several EVs (including height and AGB) can be predicted at least to the end of the current rotation and hindcasting of the states of the forest can also be undertaken, as demonstrated in this study. EODESM therefore provides a framework which can facilitate ongoing robust and consistent monitoring of the MMFR to better support sustainable use and management.

5.3. Implications for management

EODESM provides a new approach to ongoing monitoring, historical referencing and prediction of EVs and land covers that is applicable to the MMFR but also other mangrove sites either under similar management or where this is proposed in the future. The rotational cycle of timber harvesting, regrowth and maturing were tracked and described using an evidence-based approach that integrated EVs retrieved or extrapolated from optical, X-band interferometric SAR and L-band SAR data. This study, which builds on Lucas et al. (2020), provides key relationships between EVs and forest age that can be applied each time a new image in acquired with these then used to update the mapping. The EO data that allow update are currently freely available and include the Landsat but also Sentinel-2 optical sensors, although observations from these may be limited by persistent cloud. For this reason, currently operating (ALOS-2 PALSAR-2) and future L-band SAR are recommended as these provide the cloud-free observations needed to detect clearances and also have sensitivity to relative amounts of woody debris.

The approach developed is based on 10 or 30 m spatial resolution data and hence detailed information on forest dynamics (e.g., succession during different growth phases, dieback and degradation through lightning strikes) are not able to be easily discerned. This requires the use of higher spatial resolution (primarily optical and/or LIDAR) spaceborne and airborne data. This is recommended given the additional information obtained on the states and dynamics of mangroves, whether in rotational management or in protective reserves. Tracking the rotational cycle through integration of satellite-derived EVs provides forest managers with a quantitative and transferable approach for describing the state and condition of the productive mangrove zones for any point in time. However, further validation of EVs retrieved from the EO data and also derived maps of land cover and change is recommended, including through the use of

mobile applications and drones. Of note is that the classifications can be improved by simply replacing refined estimates of EVs with those used in this study if these are proven to be more robust. Hence, EODESM offers the potential for continuous improvement in monitoring capability as new information is obtained. Quantitative information on other EVs (e.g., species, water related), including in the adjoining terrestrial landscapes, could also be obtained in order to refine and extend the land cover classifications.

EODESM also has potential application for detecting change in unmanaged and natural mangroves. For example, quantitative (areal extent) and qualitative (plant species composition and functional) degradation of land covers can be detected as well as change processes. These might include identifying conversions (whether legal or illegal) of mangroves into other land uses (Richards and Friess, 2016), pinpointing selective cutting in unmanaged forests (Hirschmugl et al., 2014), or detecting cryptic ecological degradation (Dahdouh-Guebas *et al.*, 2005). As with existing or planned managed areas, this could be achieved by exploiting the same satellite sensor data used in this study, with this ideally supported by ground-based or aerial (including drone) measurements or observations and undertaken as part of a multi-scale strategy. The approach also has considerable potential for planning and/or monitoring programs aimed at restoring mangroves, including in Southeast Asia (Proisy et al., 2018; Ilman et al., 2016).

The estimates of forest age are based only on those coupes that have been cleared since the commencement of Landsat acquisitions and their availability. However, the rotational cycle of production for the MMFR is 30 years and so it was assumed that when forests were cleared, they were this age. On this basis, their age in preceding years was able to be estimated back

to 1958 but this could be extended to the start of the logging activities if the rotational cycle was adhered to. However, this needs to be evaluated against the earliest records of logging from the MMFR, which is the subject of ongoing research. Similarly, future predictions of forest age and also canopy height and AGB can be made, which can assist management planning.

Whilst the approach has been applied to managed mangroves, it is also relevant for describing the progression in natural settings, although forest age can only realistically be quantified where observations prior to colonisation are available. For forests growing prior to 1985, ageing forests is difficult from the Landsat series as data were only captured from this year. However, reference could be made to, for example, pre-1985 Landsat Multispectral Scanner System (MSS) data or aerial photography.

6. Conclusions

The study has established that EODESM provides a robust framework for quantifying current, past and future dynamics of the commercially harvested mangroves of the MMFR. Descriptors of mangroves through their rotational cycle were obtained at least annually for the MMFR between 1988 and 2016 from quantitative measures of EVs retrieved from time-series of optical and radar satellite sensor data. Of these, canopy cover was retrieved directly from the Landsat NDMI, forest age was determined from observations of clear felling during the observation period, and canopy height was estimated based on a relationship established with forest age and the 2015 TanDEM-X CHM. AGB was estimated from canopy height and extrapolated through the time series using relationships with age. On the assumption that forests are managed on a 30-year rotation, the age of forests and associated estimates of EVs were estimated prior to 1988 and beyond 2016. The close correspondence between canopy height estimated indirectly

from forest age and directly from the SRTM for 2000 confirmed reliable estimation of age and associated EVs from the EO datasets. From the range of EVs generated, land cover classifications were generated using EODESM and according to the FAO LCCS. Comparison of the resulting land cover components (e.g., mangrove lifeform, canopy height and cover) and additional descriptors (AGB, age, woody debris) allowed evidence of pre-defined change events (i.e., cutting) and processes (decomposition and removal of woody debris, forest growth) to be gathered, with this assisting mapping of these processes.

Whilst EODESM has been applied to medium resolution imagery, it can be applied at any scale because of its use of EVs with unit measures (i.e., time, m, Mg ha^{-1}, %). This opens opportunities for use at higher spatial resolution and over a range of mangrove situations. Multi-scale comparison of data acquired, including at the ground level and from drones, can also be used for validation purposes. The advantage of the approach is that EVs generated using different algorithms can be substituted into the classification. In the immediate future, integration of the Sentinel-2 optical and L-band SAR is recommended, given their sensitivity to a range of EVs including those relating to the foliar and woody components of vegetation.

EODESM has potential to assess the sustainability of production and assist future planning and management as well as conservation activities. As EODESM relies entirely on EVs retrieved from satellite sensor data, there is considerable potential for its application in other mangrove regions within and outside of Malaysia and is recommended for some areas where logging is ongoing or proposed.

Funding

Author Contributions

The MAMAForest Project Team (Lucas, Otero, Van De Kerchove, Dahdouh-Guebas and Satyanarayana) conceptualised the research and contributed towards the analysis and interpretation of the EO datasets. The analysis of the interferometric SAR data was undertaken in conjunction with Lagomasino and Fatoyinbo.

References

Alongi, D.M. (2008). Mangrove forests: Resilience, protection from tsunamis, and responses to global climate change. Estuarine, Coastal and Shelf Science 76, 1 -13.

Alongi, D.M. (2012). Carbon sequestration in mangrove forests. Carbon Management 3, 313-322.

Ariffin, R. and Mustafa N.M.S.N. (2013). A Working Plan for the Matang Mangrove Forest Reserve, Perak (6th revision). Malaysia: State Forestry Department of Perak.

Ashton EC, Hogarth PJ, Ormond R (1999) Breakdown of mangrove leaf litter in a managed mangrove forest in Peninsular Malaysia. Hydrobiologia 413: 77–88.

Aziz, A.A.. Phinn, S., Dargusch, P., Omar, H. and Arjasakusuma, S. (2015). Assessing the potential applications of Landsat image archive in the ecological monitoring and management of a production mangrove forest in Malaysia. Wetlands Ecol Manage 23, 1049-1066.

Bosire, J.O., Dahdouh-Guebas, F., Walton, M., Crona, B.I., Lewis III., R.R., Field. C., Kairo, J.G. and Koedam, N. (2008). Functionality of restored mangroves: A review. Aquatic Botany 89, pp. 251 - 259.

Bunting, P., Clewley, D., Lucas, R.M. and Gillingham, S. (2013). The Remote Sensing and GIS Software Library (RSGISLib). *Computers and Geosciences*, 62, 206-226

Bunting, P., Rosenqvist, A., Lucas, R.M., Rebelo, L, Hillardes, L, Thomas, N., Hardy, A., Itoh, T., Shimada, S. and Finlayson, C.M. (2018). The Global Mangrove Watch – A new 2010 global baseline of mangrove extent. Remote Sensing, 10, 1669.

Chong, V.C. (2006). Sustainable utilization and management of mangrove ecosystems of Malaysia. Aquatic Ecosystems Health and Management 9 (2), 249 - 260.

Clewley, D., Bunting, B., Shepherd, J., Gillingham, S., Flood, N., Dymond, J., **Lucas, R**., Armston, J. and Moghaddam, M. (2014). A python-based open source system for geographic object-based image analysis (GEOBIA) utilising raster attribute tables. *Remote Sensing* 6 (7), 6111-6135.

Costanza, R., d'Arge, R., de Groot, R., Farber, S., Grasso, M., Hannon, B., Limburg, K., Naeem, S., O'Neill, R.V., Paruelo, J., Raskin, R.G., Sutton, P. and van den Belt, M. (1997). The value of the world's ecosystem services and natural capital. Nature 387(6630): 253–260.

Dahdouh-Guebas, F., Hettiarachchi, S., Sooriyarachchi, S., Lo Seen, D., Batelaan, O., Jayatissa, L.P. & Koedam, N. (2005). Transitions in ancient inland freshwater resource management in Sri Lanka affect biota and human populations in and around coastal lagoons. Current Biology 15(6): 579-586.

Di Gregorio, A. (2016). Land Cover Classification System. Software version 3. Food and Agriculture Organization of the United Nations. Available online http://www.fao.org/3/a-i5232e.pdf [May 2019]

Di Gregorio, A. and Jansen, L.J.M. (2000). Land Cover Classification System (LCCS): Classification Concepts and User Manual. Environment and Natural Resources Service, GCP/RAF/287/ITA Africover - East Africa Project and Soil Resources, Management and Conservation Service. 179 pages, 28 figures, 3 tables and including CD-ROM. FAO, Rome. 2000.

Di Nitto, D., Neukermans, G., Koedam, N. Defever, H. Pattyn, F., Kairo , J.G. and Dahdouh-Guebas (2014). Mangroves facing climate change: landward migration potential in response to projected scenarios of sea level rise. Biogeosciences 10: 857-871.

Duke, N.C., Kovacs, J., Griffiths, A., Preece, L., Hill, J.E., Van Oosterzee, P., Mackenzie, J., Morning, H. and Burrows, D. (2017). Large-scale dieback of mangroves in Australia's Gulf of Carpentaria: a severe ecosystem response, coincidental with an unusually extreme weather event. Marine and Freshwater Research, 68 (10), 1816-1829.

Ellison, A. (2000). Mangrove restoration: do we know enough?. *Restoration Ecology*, vol. 8, pp. 219 – 229.

Fatoyinbo, T.E., Simard, `M., Washington-Allen, R.A. and Shugart, H.H. (2008). Landscape-scale extent, height, biomass and carbon estimation of Mozambique's mangrove forests with Landsat ETM+ and Shuttle Radar Topography Mission elevation data. *Journal of Geophysical Research*, 113, G02S06, 13p. doi:10.1029/2007JG000551

Fatoyinbo, T.E., and Simard, M. (2013). Height and biomass of mangroves in Africa from ICESat/ GLAS and SRTM. International Journal of Remote Sensing 34 (2), 668 - 681.

Fatoyinbo, T., Feliciano, E., Lagomasino, D., Lee, S. and Trettin, C. (2017). Estimating mangrove aboveground biomass from airborne LiDAR data: a case study from the Zambezi River delta. Environmental Research Letters, 13, 025012.

Gillingham, S. and Bunting, P. (2014). RFC40: Improving performance of Raster Attribute Table implementation for large tables. Available online http://trac.osgeo.org/gdal/wiki/rfc40_enhanced_rat_support [10th October, 2018].

Giri, C., Pengra, B., Zhu, A., Singh, A. and Tieszen L.L. (2007). Monitoring mangrove forest dynamics of the Sundarbans in Bangladesh and India using multi-temporal satellite data from 1973 to 2000. Estuarine, Coastal and Shelf Science 73, 91-100.

Goessens, A., Satyanarayana, B., Van der Stocken, T., Zuniga, M.Q., Mohd-Lokmabn, H., Sulong, I. and Dahdouh-Guebas, F. (2014). Is Matang Mangrove Forest in Malaysia sustainably rejuvenating after more than a century of conservation and harvesting management. PloS ONE, 9(8), e105069.

Hamdan, O., Aziz, H.K. and Hasmadi, I.M. (2014). L-band ALOS PALSAR for biomass estimation of Matang Mangroves, Malaysia. Remote Sensing of Environment, 155, 69-78.

Hirschmugl, M., Steinegger, M., Gallaun, H. and Schardt, M., 2014. Mapping Forest Degradation due to Selective Logging by Means of Time Series Analysis: Case Studies in Central Africa. Remote Sensing, 6(1), 756-775.

Huge, J., Vande Velde, K., Benitez-Capistros, F., Japay, J.H., Satyanarayana, B., Nazrin Ishak, M., Quispe-Zuniga, M., Lokman, B.H.M., Sulong, I., Koedam, N. and Dahdouh-Guebas, F. (2016). Mapping discourses using Q methodology in Matang Mangrove Forest, Malaysia. Journal of Environmental Management 183, 988-997.

Ilman, M., Dargusch, P., Dart, P., & Onrizal (2016). A historical analysis of the drivers of loss and degradation of Indonesia's mangroves. Land Use Policy, 54, 448-459

Kairo, J.G., Dahdouh-Guebas, F., Bosire, J. and Koedam, N. (2001). Restoration and management of mangrove ecosystems - a lesson for and from the East African region. South African Journal of Botany 67, 383-389.

Koedam, N. and Dahdouh-Guebas, F. (2008). Ecological quality changes precede changes in quantity in mangrove forests. Science (E-Letter: 02/10/2008).

Komiyama, A., Ong, J. E., & Poungparn, S. (2008). Allometry, biomass, and productivity of mangrove forests: A review. Aquatic Botany, 89, 128–137.

Lee, S.Y., J.H. Primavera, F. Dahdouh-Guebas, K. McKee, J.O. Bosire, S. Cannicci, K. Diele, F. Fromard, N. Koedam, C. Marchand, I. Mendelssohn, N. Mukherjee, S. Record. (2014).

Ecological role and services of tropical mangrove ecosystems: A reassessment. Global Ecology and Biogeography 23: 726–743.

López-Portillo, J., Lewis III, R.R, Saenger, P., Rovai, A., Koedam, N., Dahdouh-Guebas, F., Agraz-Hernández, C. and Rivera-Monroy, V.H. (2017). Mangrove Forest Restoration and Rehabilitation. In Mangrove Ecosystems: A Global Biogeographic Perspective. https://doi.org/10.1007/978-3-319-62206-4_10

Lucas, R. M.; Clewley, D.; Accad, A.; Butler, D.; Armston, J.; Bowen, M.; Bunting, P.; Carreiras, J.; Dwyer, J.; Eyre, T. (2014). Mapping forest growth and degradation stage in the Brigalow Belt Bioregion of Australia through integration of ALOS PALSAR and Landsat-derived foliage projective cover data. *Remote sensing of environment*, *155*, 42–57.

Lucas, R.M. and Mitchell, A.L. (2017). Integrated land cover and change classifications. In: The Roles of Remote Sensing in Nature Conservation (Eds. Ricardo Díaz-Delgado, Richard Lucas, Clive Hurford), 11, pp. 295-308.

Lucas, R.M., Mueller, N., Siggins, A., Owers, C., Clewley, D., Bunting, P., Kooymans, C., Tissott, B., Lewis, B., Lymburner, L and Metternicht, G. (2019). Land cover mapping using Digital Earth Australia, Data, 4(4), 143.

Lucas, R.M., Van De Kerchove, R., Otero, V., Lagomasino, D., Fatoyinbo, L., Satyanarayana, B. and Dahdouh-Guebas, F. (2020). Structural characterisation of mangrove forests achieved

through combining multiple sources of remote sensing data. Remote Sensing of Environment, 237, 111543.

Luckman, A., Baker, J., Honzak, M. and Lucas, R.M. (1998). Tropical forest biomass density estimation using JERS-1 SAR: Seasonal variation, confidence limits, and application to image mosaics. Remote Sensing of Environment, 63, 2, 126-139.

Muda, A. & N.M.S. Nik Mustafa, 2003. A Working Plan for the Matang Mangrove Forest Reserve, Perak. Fifth Revision. State Forestry Department, Perak Darul Ridzuan. 320 pp.

Murray, N.J., Phinn S., DeWitte, M., Ferrari, R., Johnston, R., Lyons, M.B., Clinton, N., Thau, D. and Fuller, R.A. (2019). The global distribution and trajectory of tidal flats. Nature565, 222-225.

Noakes, D.S.P. (1952). A working plan for the Matang mangrove Forest Reserve Perak. Forest Department, Federation of Malaya. 178 pp.

Otero, V., Van De Kerchove, R., Satyanarayana, B., Martínez-Espinosa, C., Bin Fisol, M.A., Bin Ibrahim, M.R., Ibrahim S., Husain, M.L. Lucas, R. and Dahdouh-Guebas, F. (2018). Managing mangrove forests from the sky: Forest inventory using field data and Unmanned Aerial Vehicle (UAV) imagery in the Matang Mangrove Forest Reserve, peninsular Malaysia. Forest Ecology and Management 411, 35 - 45.

Otero, V., Van De Kerchove, R., Satyanarayana, B., Mohd-Lokman, M., Lucas, R. and Dahdouh-Guebas, F. (2019). An Analysis of the Early Regeneration of Mangrove Forests using

Landsat Time Series in the Matang Mangrove Forest Reserve, Peninsular Malaysia. Remote Sensing 11 (7), 774.

Pastor-Guzman, J., Dash, J. and Atkinson, P. (2018). Remote sensing of mangrove forest phenology and its environmental drivers. Remote Sensing of Environment, 2015, 71-84.

Proisy, C., Viennois, G., Sidik, F., Andayani, A., Enright, J.A., Guitet, S., Gusmawati, N., Lemonnier, H., Muthusankar, G., Olagoke, A., Prosperi, J., Rahmania, R., Ricout, A., Soulard, B., & Suhardjono (2018). Monitoring mangrove forests after aquaculture abandonment using time series of very high spatial resolution satellite images: A case study from the Perancak estuary, Bali, Indonesia. Marine Pollution Bulletin, 131, 61-71.

Richards, D.R. and Friess, D.A. (2016). Rates and drivers of mangrove deforestation in Southeast Asia, 2000–2012. PNAS 113 (2), 344-349.

Rönnbäck, P., Crona, I., and Ingwall, L. (2007). The return of ecosystem goods and services in replanted mangrove forests: perspectives from local communities. Environmental Conservation 4, 313 – 324.

Satyanarayana B., Bhanderi P., Debry M., Maniatis D., Foré F., Badgie D., Jammeh K., Vanwing T., Farcy C., Koedam N. and Dahdouh-Guebas F. (2012). A socio-ecological assessment aiming at improved forest resource management and sustainable ecotourism development in the mangroves of Tanbi Wetland National Park, The Gambia, West Africa. Ambio 41, 513-26. doi: 10.1007/s13280-012-0248-7.

Satyanarayana, B., T. Van der Stocken, G. Rans, K.A.S. Kodikara, G. Ronsmans, L.P. Jayatissa, H. Mohd-Lokman, N. Koedam & F. Dahdouh-Guebas, 2017. Island-wide coastal vulnerability assessment of Sri Lanka reveals that sand dunes, planted trees and natural vegetation may play a role as potential barriers against ocean surges. Global Ecology and Conservation 12: 144-157.

Shimada, M., Isoguchi, O., Tadono, T., & Isono, K. (2009). PLASAR radiometric calibration and geometric calibration. IEEE Transaction on Geosciences and Remote Sensing, 3, 765–768.

Sillanpaa, M., Vantellingen, J. and Friess. D.A. (2017). Vegetation regeneration in a sustainably harvested mangrove forest in West Papua, Indonesia. Forest Ecology and Management 390, 137 - 146.

Simard, M., Fatoyinbo, L., Smetanka, C., Rivera-Monroy, V.H., Castañeda-Moya, E., Thomas, N and Van de Stocken, T., 2018. Mangrove canopy height globally related to precipitation, temperature and cyclone frequency. Nature Geoscience, 12, 40-45. https://doi.org/10.1038/s41561-018-0279-1

Simard, M., Fatoyinbo, L., Smetanka, C., Rivera-Monroy, V.H., Castañeda-Moya, E., Thomas, N. and Van der Stocken, T. (2019). Mangrove canopy height globally related to precipitation, temperature and cyclone frequency. Nature Geoscience 12, 40-45.

Spalding, M., M. Kainuma & L. Collins, 2010. Word Atlas of Mangroves. Earthscan, London: 319

Tarantino, C., Adamo, M., Lucas, R.M. and Blonda, P. (2016). Detection of changes in semi-natural grasslands by Cross Correlation Analysis with Worldview-2 images and new Landsat-8 data. Remote Sensing of Environment, 175, 65-72.

Thomas, N., Lucas, R., Bunting, P., Hardy, A., Rosenqvist, A. and Simard, M. (2017). Distribution and drivers of global mangrove forest change, 1996–2010. PLoS ONE 06/2017; 12(6): e0179302.

Tomlinson, P.B (1986). The botany of mangroves. Cambridge University Press, UK. pp. 173-382.

Verbesselt, J., Hyndman, R., Newnham, G., Culvenor, D. (2010). Detecting trend and seasonal changes in satellite image time series. Remote Sens. Environ., 114, 106–115.

Walters, B.B., Rönnbäck, P., Kovacs, J.M., Crona, B., Hussain, S.A., Badola, R., Primavera, J.H., Barbier, E. and Dahdouh-Guebas, F. Ethnobiology, socio-economics and management of mangrove forest: A review. Aquatic Botany, vol. 89, pp. 220 – 236, 2008.

Walton, M.E.M., Samonte-Tan, G.P.B., Primavera, J.H., Edwards-Jones G. and Le Vay, L. (2006). Are mangroves worth replanting? The direct economic benefits of a community-based reforestation project. Environmental Conservation 33 (4), 335-343. doi:10.1017/S0376892906003341

Weidmann, Nils B., Doreen Kuse, and Kristian Skrede Gleditsch (2010). The Geography of the International System: The CShapes Dataset. International Interactions 36 (1).

Worthington, T., and Spalding, M. (2018). Mangrove Restoration Potential: A global map highlighting a critical opportunity. https://doi.org/10.17863/CAM.39153

Table 1. Relationships describing the trends in biophysical variables with age.

No.	Equation	y	x	R^2	n
1	$y = -0.015(x^2) + 1.1412x^4$	[1]CHM (m)	[2]Age (Years)	0.92	331
2	$y = 91.369\ln(x) - 95.839$	[3,4]AGB (Mg ha^{-1})	Age (Years)	0.88	166
3	$y = -0.0187x + 146.17$	[5]L_{HH} DN	% Decomp	0.74	292

[1]RMSE of 1.94 m in estimation of canopy height from TanDEM-X when compared to CHMs generated from DJI Phantom RGB images (Lucas et al. 2020).
[2]Typical errors in the estimation age ± 6 months for all age classes (Lucas et al., 2020).
[3]RMSE of 148 Mg ha^{-1} for SRTM-retrieved AGB based on Simard et al. (2018), RSME of 79 Mg ha^{-1} based on comparison with ground data from the MMFR.
[4]For forests older than 3 years
[5]Indicates relative amounts of woody debris amounts.

Figure Captions.

Figure 1. The location of the Matang Mangrove Forest Reserve (MMFR) in Peninsular Malaysia. Map adapted from Weidmann *et al.* (2010).

Figure 2. The 98 acquisition dates of JERS-1 SAR (1993-1997), ALOS PALSAR (2006-2011) and ALOS-2 PALSAR-2 (2015-2016) (grey) and Landsat sensor data (white) acquired for the MMFR. The numbers represent the dates of image acquisition. Landsat sensor and ALOS PALSAR data were acquired on the 1st March 2018. ALOS PALSAR data were also acquired on the 29th Apr 2009, 30th Aug and 30th Nov 2007, 14th and 18th March 2009, 5th 14th and 22nd Dec 2019, 25th Dec 2010 and 23rd Jan 2011. The dates of acquisition SRTM, TanDEM-X and Worldview-2 data were the 11th and 22nd February, 2000, mid 2015 (actual date unknown) and 23rd January, 2016 respectively.

Figure 3. The LCCS Taxonomy (Taken from Di Gregorio and Jansen, 2000; Di Gregorio, 2016).

Figure 4. Flow chart outlining the steps taken to generate land cover and evidence-based change maps for the MMFR, with this involving generation of age class maps through time-series comparison of Japanese L-band SAR and Landsat sensor data (green arrows), retrieval of EVs from these (i.e., canopy cover and relative amounts of woody debris) and also interferometric SAR (orange), the use of relationships between age and both canopy height and AGB to estimate these variables for each observation date (blue), integration of all EVs to generate land cover classifications and descriptions and evidence-based change maps (purple). The SRTM CHM was used to validate the age and canopy height estimates for 2000.

Figure 5. Estimates of canopy cover (%) and b) lifeform (physiognomic aspect of trees based on upper canopy height) generated for the MMFR, September 29th 2016. Coordinates are for Universal Transverse Mercator (UTM) Zone 47 N.

Figure 6. Observed a) increase in above ground biomass (Mg ha^{-1}; derived from the TX$_{CHM}$), b) decrease in LHH (DN) following clearance of mature production forests, and c) Relationship between L-band HH (Digital number DN) and the relative decomposition of woody material (%).

Figure 7. Example temporal maps of EVs generated for the MMFR. a) and b) Forest age, c) canopy height (m) and c) above ground biomass (Mg ha^{-1}) for four selected years.

Figure 8.   Progressive increase in the area of mangrove forest cleared in the productive zone and the rates of change between different observation times.

Figure 9.   LCCS Level 4 classifications of the MMFR for a) 30th July 2000 and b) 29th September 2016.   Each image is associated with a Raster Attribute Table (RAT) that contains information on mangrove forest age (days or years since clearing), AGB (Mg ha-1), canopy cover (%) and height (m) and lifeform.   Additional information on, for example, the amounts of woody debris (relative %), dominant plant species, water states, movement and turbidity, can be included.

Figure 10.   Canopy height estimated for 2000 from a) age (estimated for the 30th July 2000) and b) SRTM data acquired between the 11th and 22nd February, 2000.   c) Comparison of estimates for different age bins of 1 year (RMSE = 5.28 m, n = 438).

Figure 11.   Changes a) between LCCS Level 3 categories (natural aquatic vegetation (i.e., mangroves) and bare surfaces) and b) within LCCS 4 category canopy height classes (defined by the FAO LCCS).   Note that a height value is not associated with regrowth in 2016 as this is a between class change. Some forests have also been cut and have subsequently regrown between the two dates. The products are generated from a comparison of classifications for 30th July 2000 and 29th September 2016.   Areas that have been clear cut on or just before 29th September 2019 and regrowing on areas that were identified as cleared on the 30th July 2000 are highlighted.   All image products are projected to Universal Transverse Mercator (UTM) Zone 47 North.

Figure 12. An overview of a typical logging cycle, which takes place over approximately 30 years, and its description using combinations of environmental variables retrieved from different sources (satellite sensors operating in different modes, knowledge).   The sequence considers clear felling (Stage I, which takes up to 2 years for each coupe), decomposition of woody debris and formation of a closed canopy (II), maturing of the forest (including thinning; III) and formation of substantive prop root systems (IV) in the *Rhizophora*-dominated forest (Lucas et al., 2019).

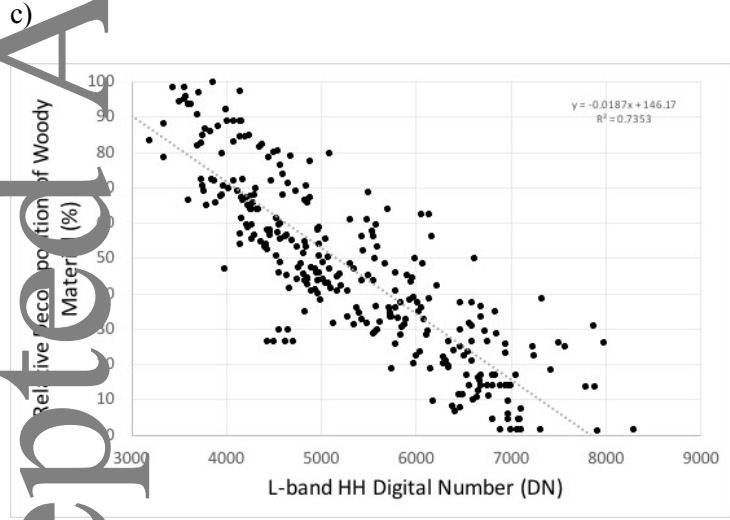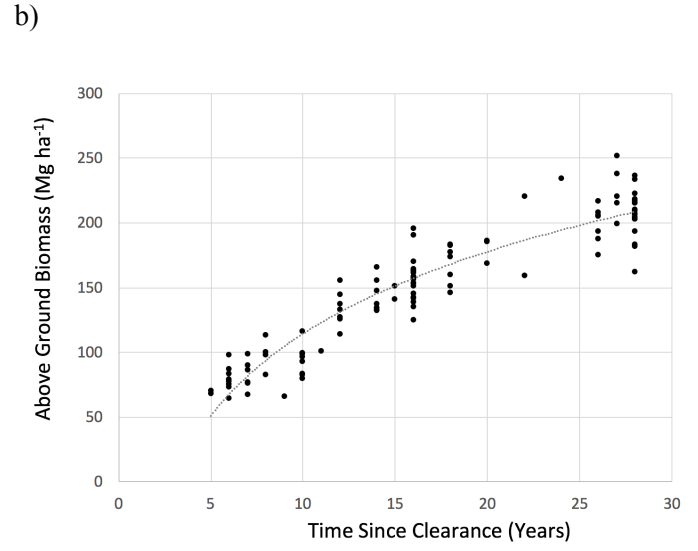|	1988	1989	1990	1991	1992	1993	1994	1995	1996	1997	1998	1999	2000	2001	2002	2003	2004	2005	2006	2007	2008	2009	2010	2011	2012	2013	2014	2015	2016
													JERS-1 SAR								ALOS PALSAR						ALOS PALSAR-2		
Jan					30		14	1		19										29		20	20	18					
Feb		22		28			27	2											6	8	1	16	16					19	18
Mar						12	24	30	16					3							1	4	7					18	
Apr			14				12		14	16											16	14		8				20	
May										30									2	25	3	30			20				
Jun					9				12										1				24				3	15	
Jul	29								26	25			30								17	20	23						
Aug							22	9		26					29					1		6	9						
Sep									8									30	1			4	7						29
Oct							5		22												12	20	23				2	1	
Nov							18													1	3		9			23			
Dec										13		27				30	16			17	19	14	8						
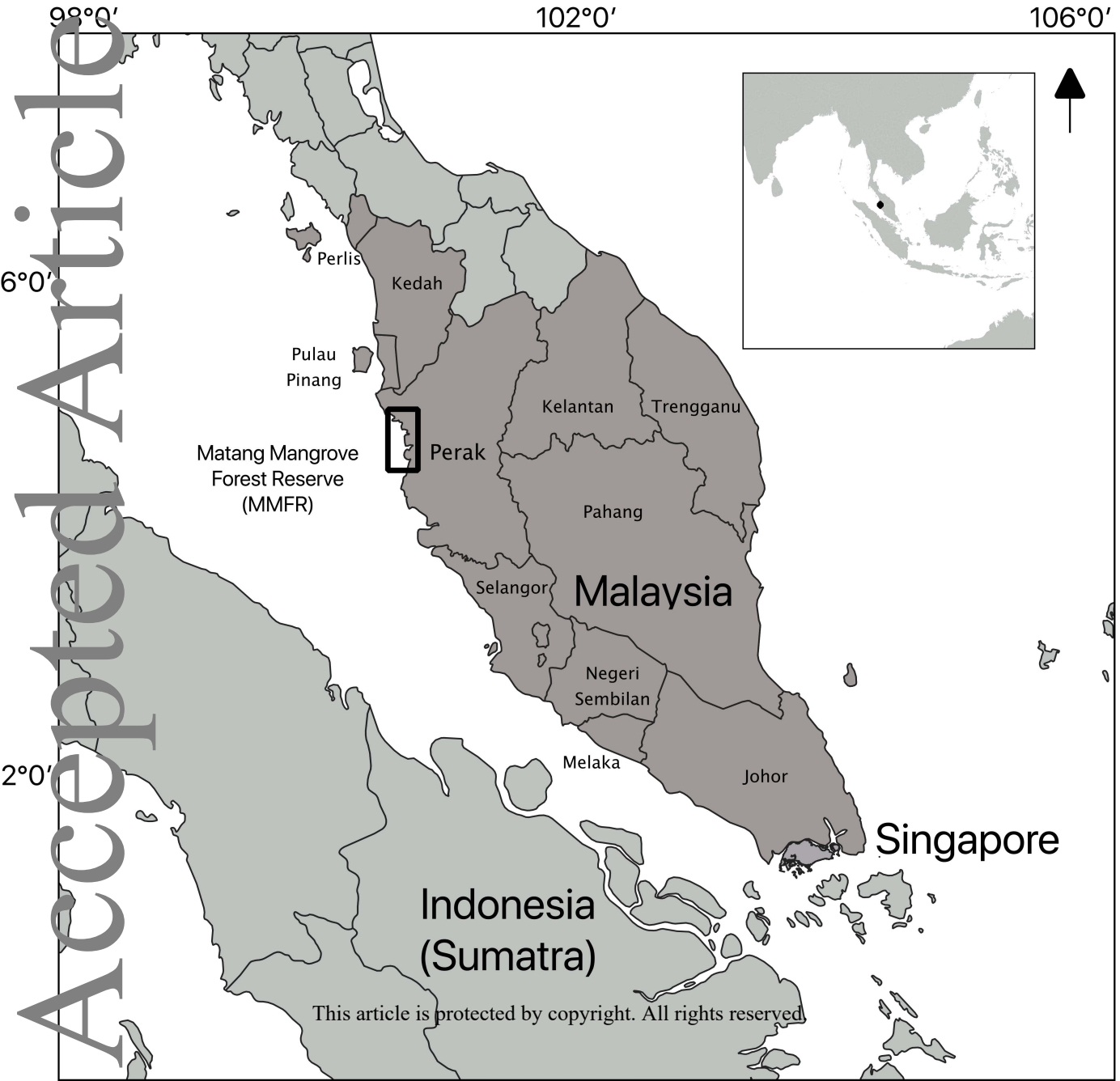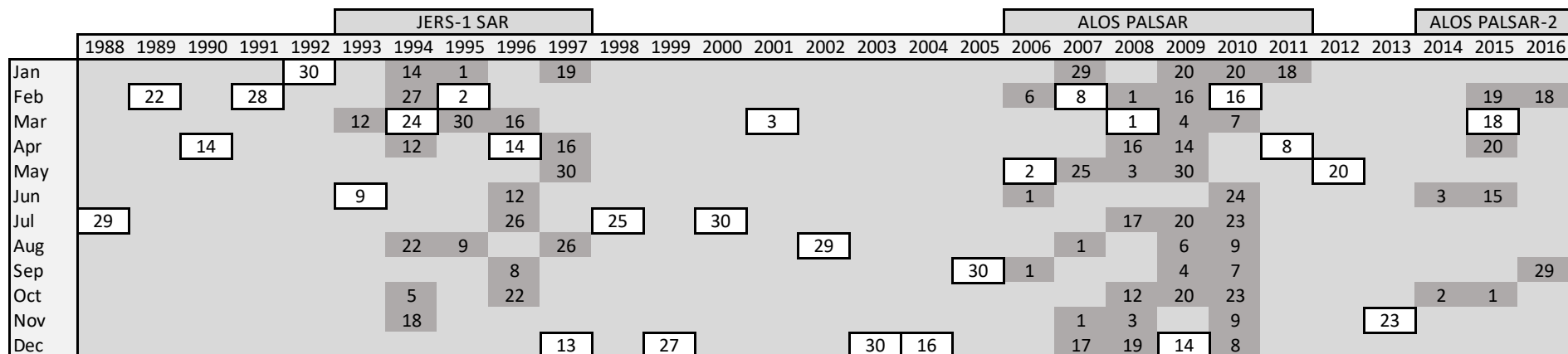
Landsat sensor and ALOS PALSAR acquired on the 1st March 2008

ALOS PALSAR acquired also on: 29 Apr 2009, 30 Aug & 30 Nov 2007, 14/18 Mar 2008, 5/14/22 Dec & 21 Sep 2009, 25 Dec 2010 and 23 Jan 2011

a)   b)

Trees > 3 – < 5 m
Trees >= 5 m

a)

b)

c)

y = -0.0187x + 146.17
R² = 0.7353
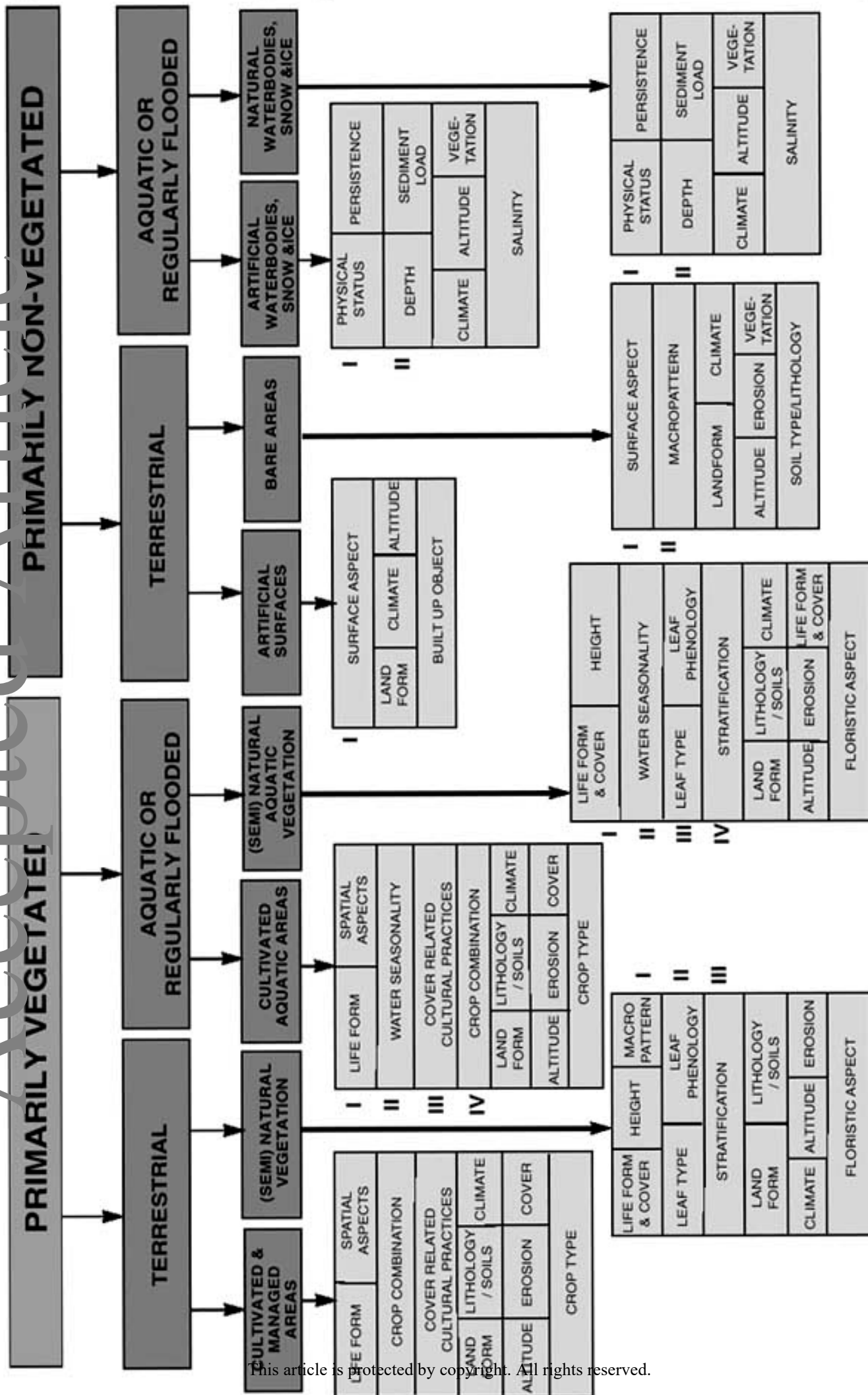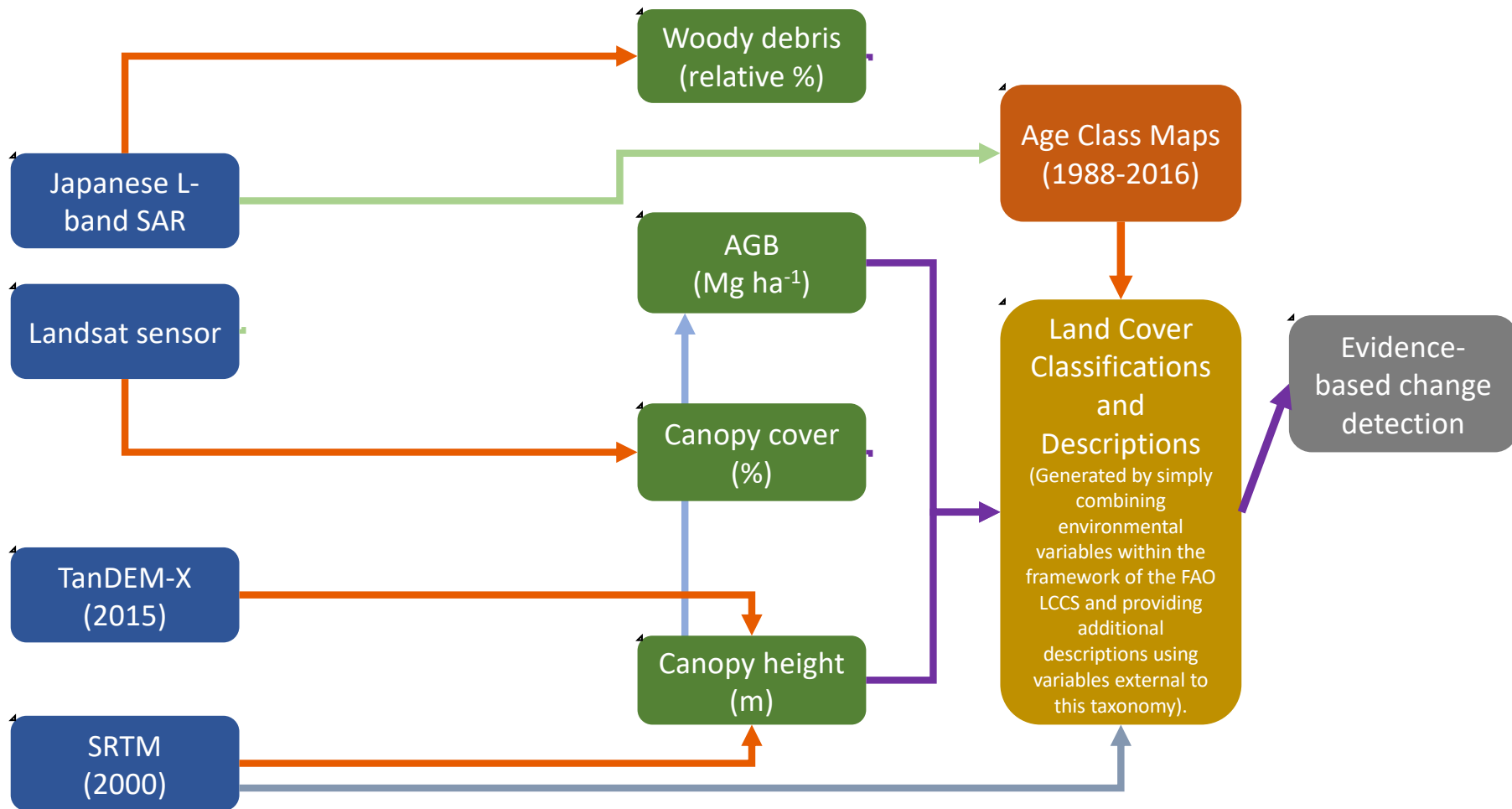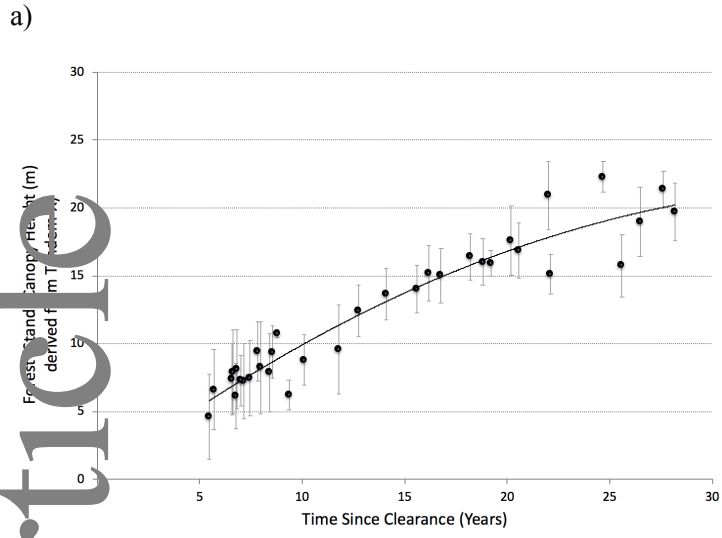
a)

666000   676000   686000

540000

530000

5200...

510000

500000

14 Apr 1990   09 Aug 1995   30 Sep 2005   15 Jun 2015

b)

1 2 3 4 5 6 7 8 9 10 11 12 13 14 15 16 17 18 19 20 21 22 23 24 25 26 27 28 29 30 31

c)

0   > 20 metres

d)

0   > 200 Mg/ha

a)

b)

665000   675000   685000

540000
530000
520000
510000
500000
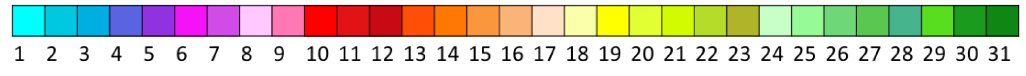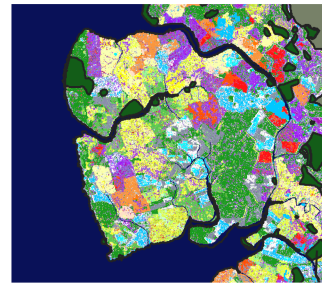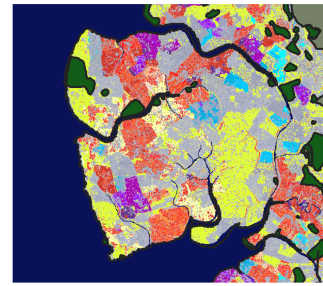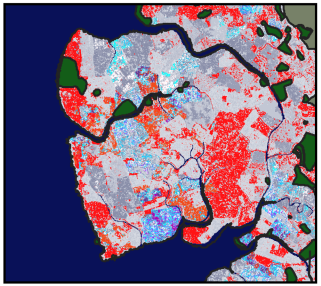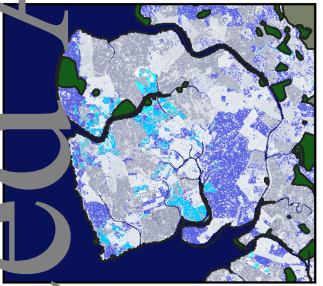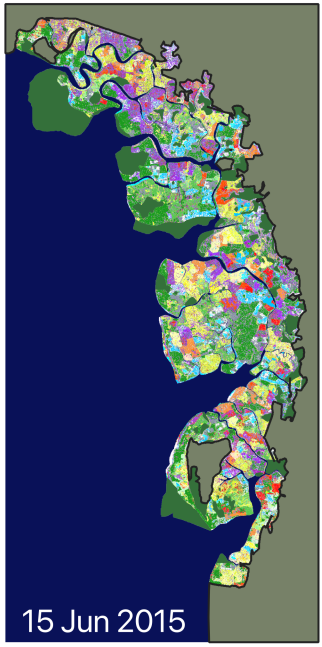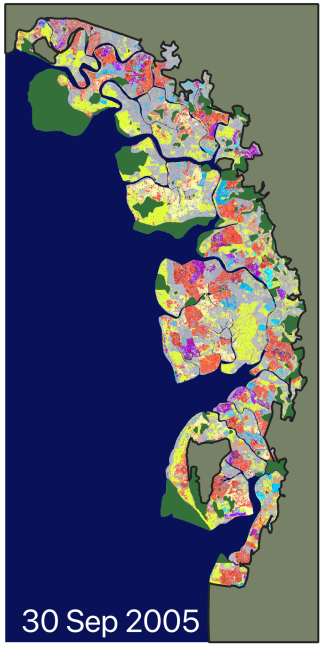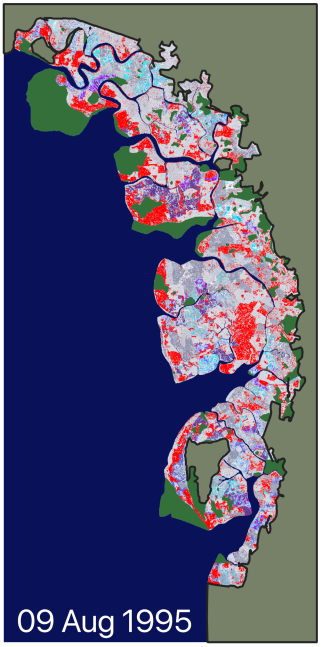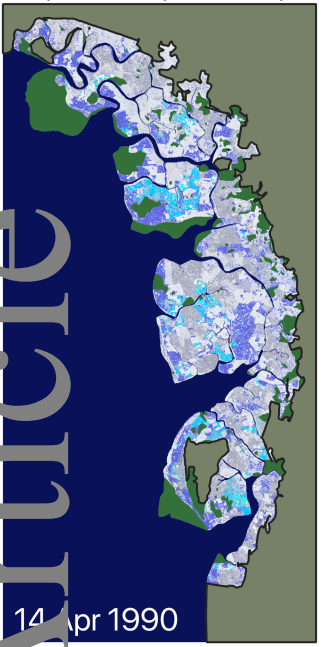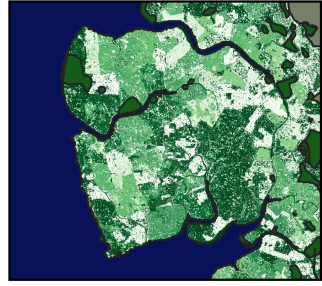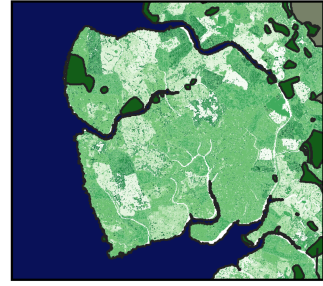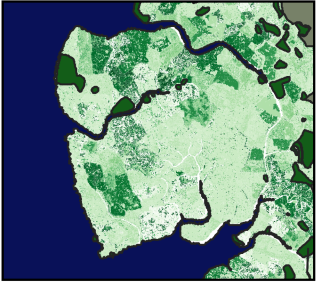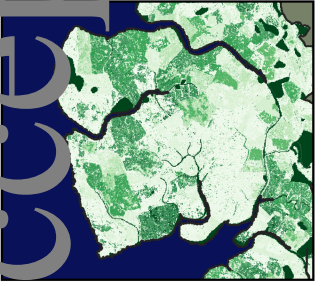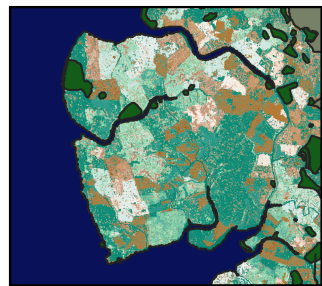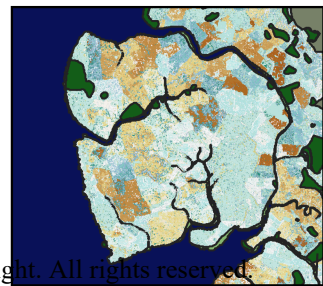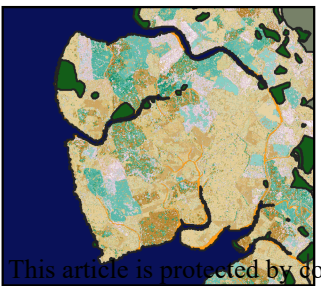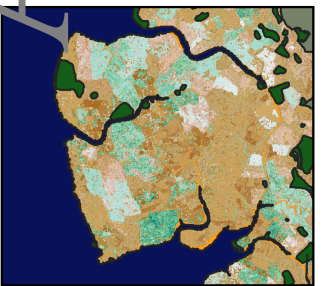
665000   675000   685000

665000   675000   685000

Canopy height

	2-3 m	5-7 m	7-14 m	>14 m
	B8	B7	B6	B5
Lifeform and canopy cover				
Scattered (1-4 %)	A16			
Sparse (4 - - 15%)	A15			
Open (15 - - 40 %)	A13			
Trees open (40 - - 65 %)	A12			
Trees closed (≥ 65%)	A10			

Terrestrial land covers
Artificial surface
Natural water

a) b)

c)

Canopy Height (m)
1 2 3 4 5 6 7 8 9 10 11 12 13 14 15 16 17 18 19 20 21

Terrestrial
Protective
Restrictive
Unproductive
Productive (mature forest)
Water

Age-derived canopy height for 30th July 2000 (m)

SRTM-derived canopy height for 11-22nd February 2000 (m)

a)
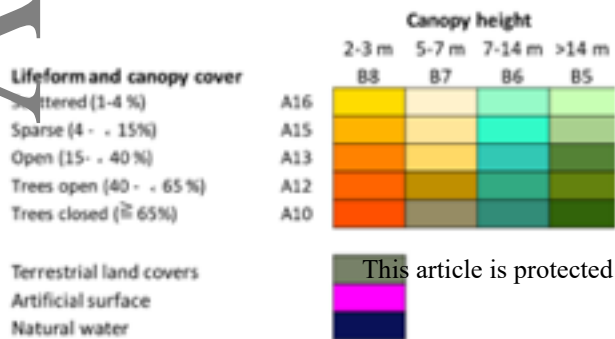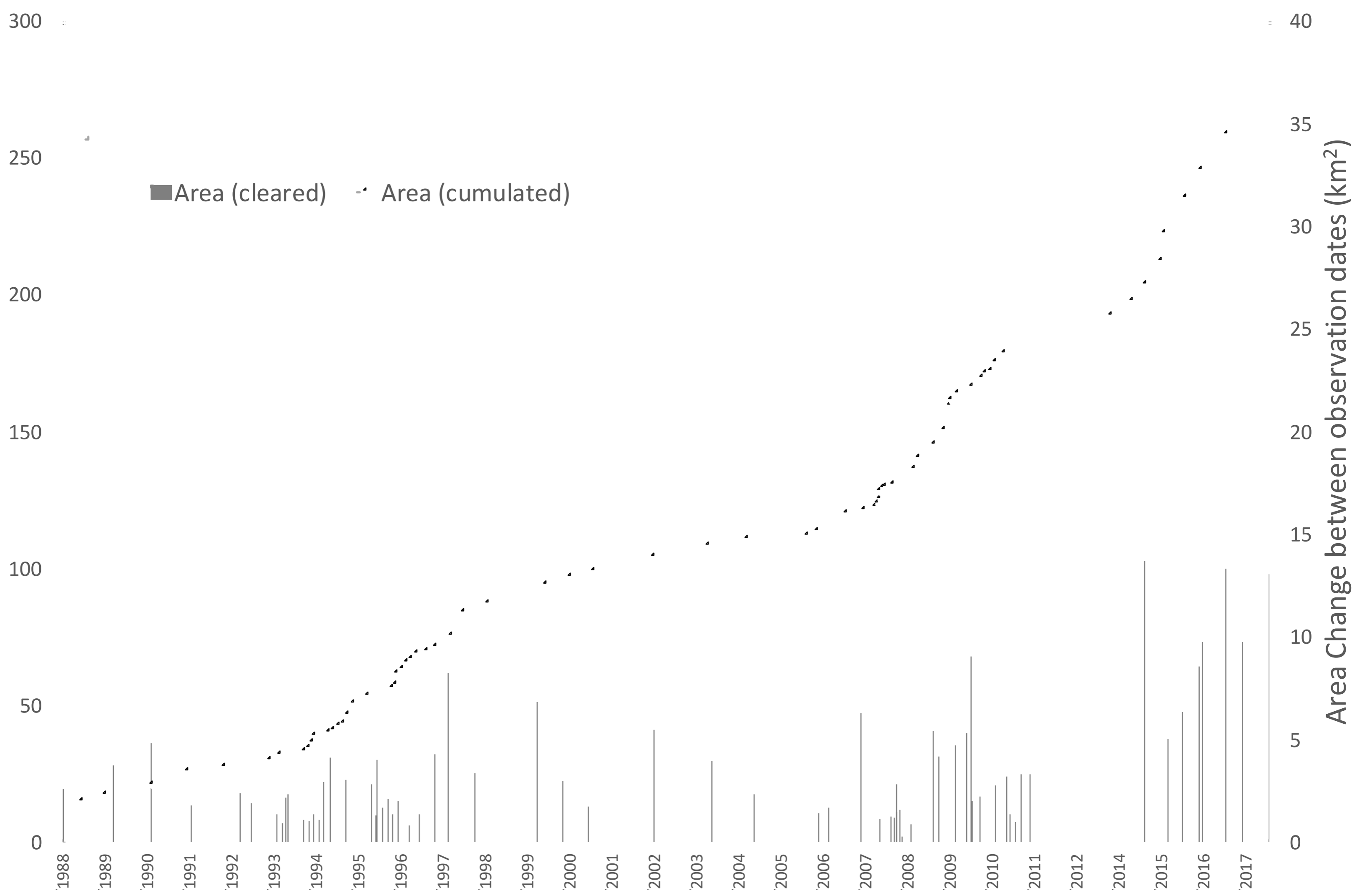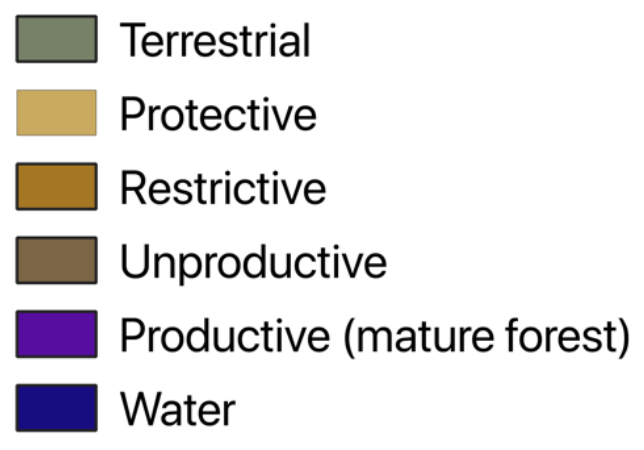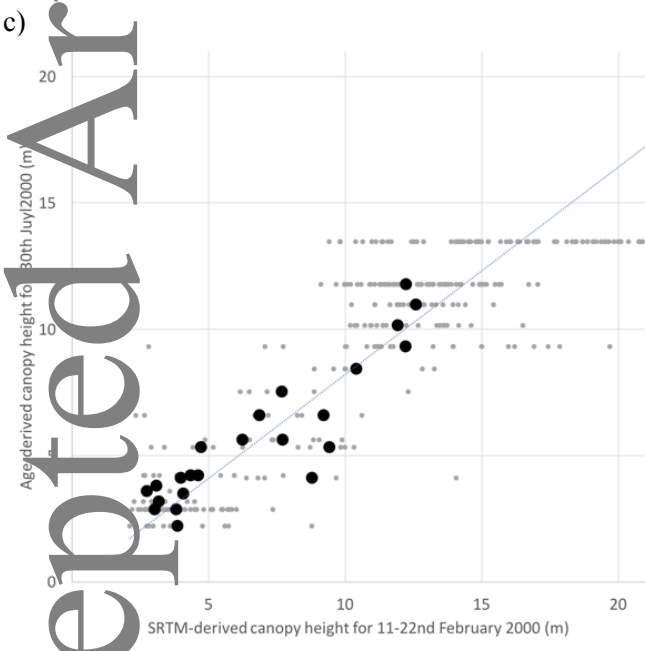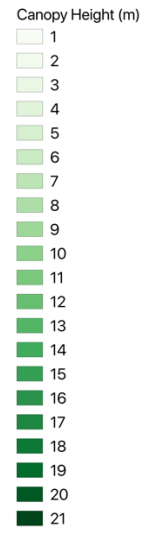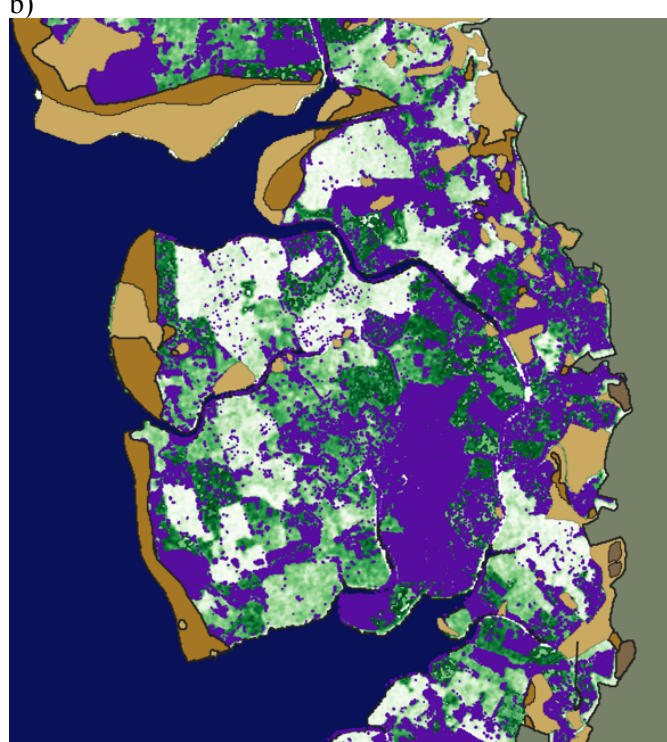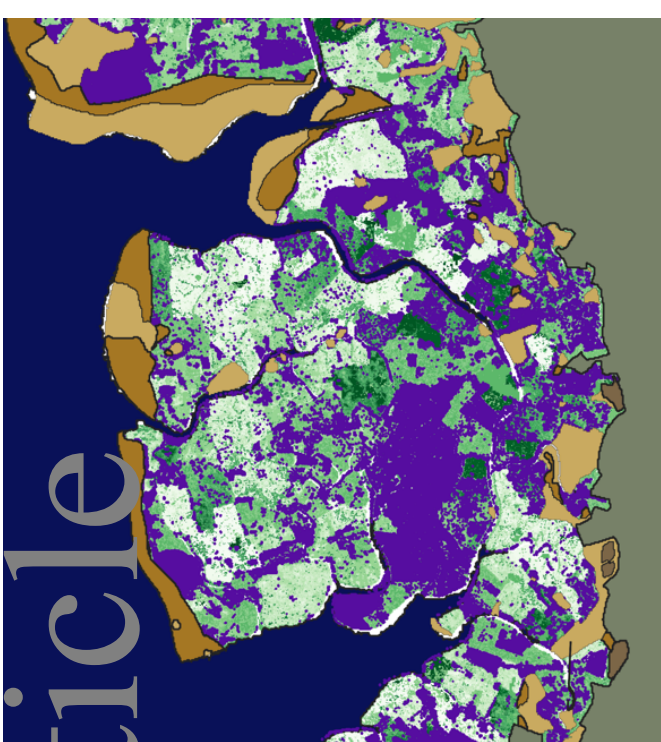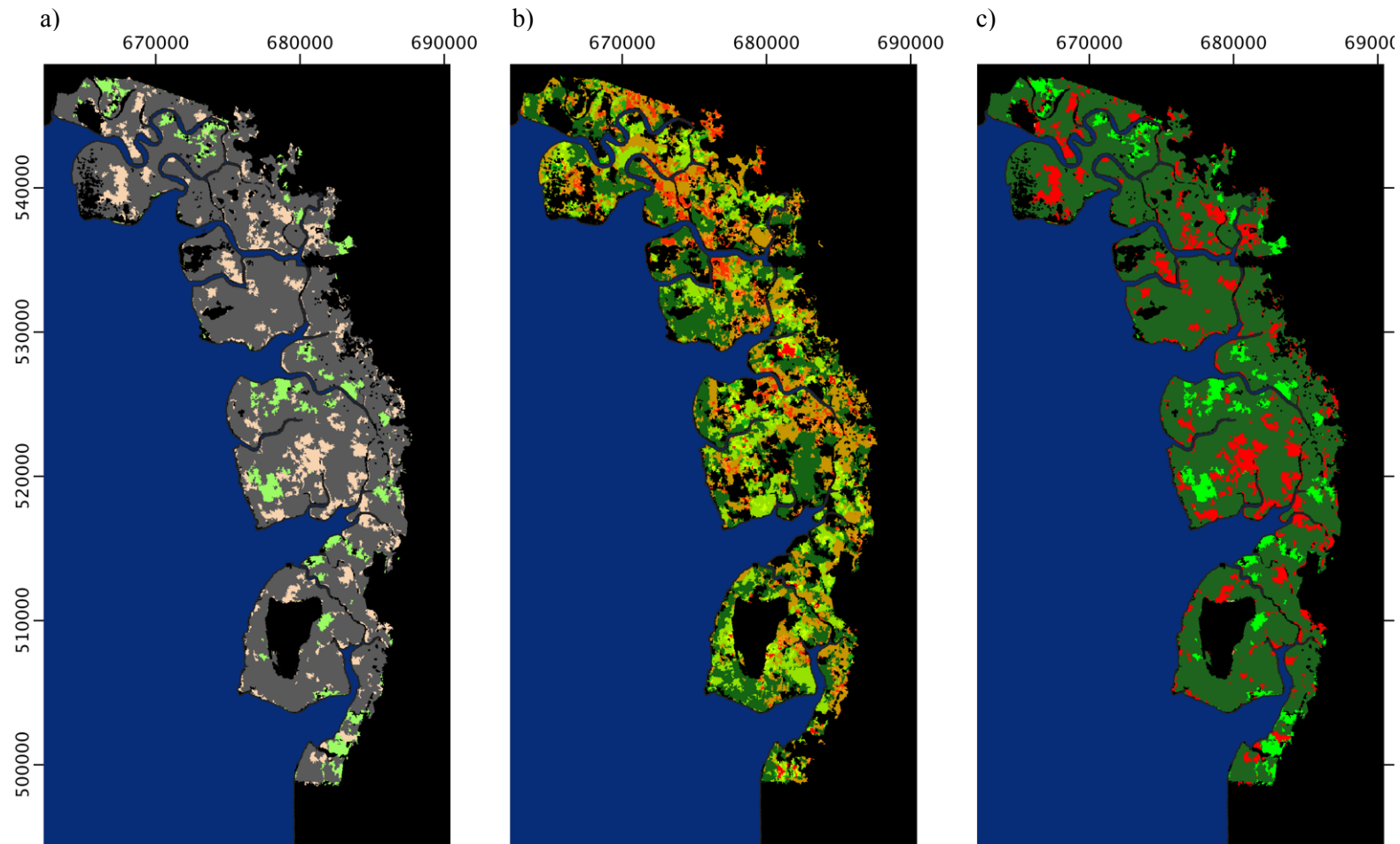
- Natural/semi-natural aquatic vegetation to naturally bare surface
- Naturally bare surface to natural/semi-natural aquatic vegetation

b)

- Remained as trees (> 14 m)
- Remained as trees (> 7-14 m)
- Trees (>3-5m) to trees (> 14 m)
- Trees (>3-5m) to trees (7-14m)
- Trees (>5-7m) to trees (7-14m)
- Trees (>5-7m) to trees (> 14m)
- Trees (>7-14m to trees (> 14m)

- Trees (>7-14m) to trees (5-7 m)
- Trees (>14m) to trees (7-14 m)
- Trees (>5-7m) to trees (7-14 m)

c)

- Clear cutting
- Regrowth

Clear Cut (Year 0)

Approx. 30 year old forest

Decomposition of woody material and formation of a closed canopy (approx. 8 years)

Stage (I-IV)
Woody debris (L-band HH)
Canopy cover (Landsat NDMI)
Canopy height (Interferometric. SAR)
Lifeform (from canopy height)
Root systems (L-band HH)
AGB (Relationship with canopy height and age)
Species (Landsat and canopy height)
Leaf type
Phenology
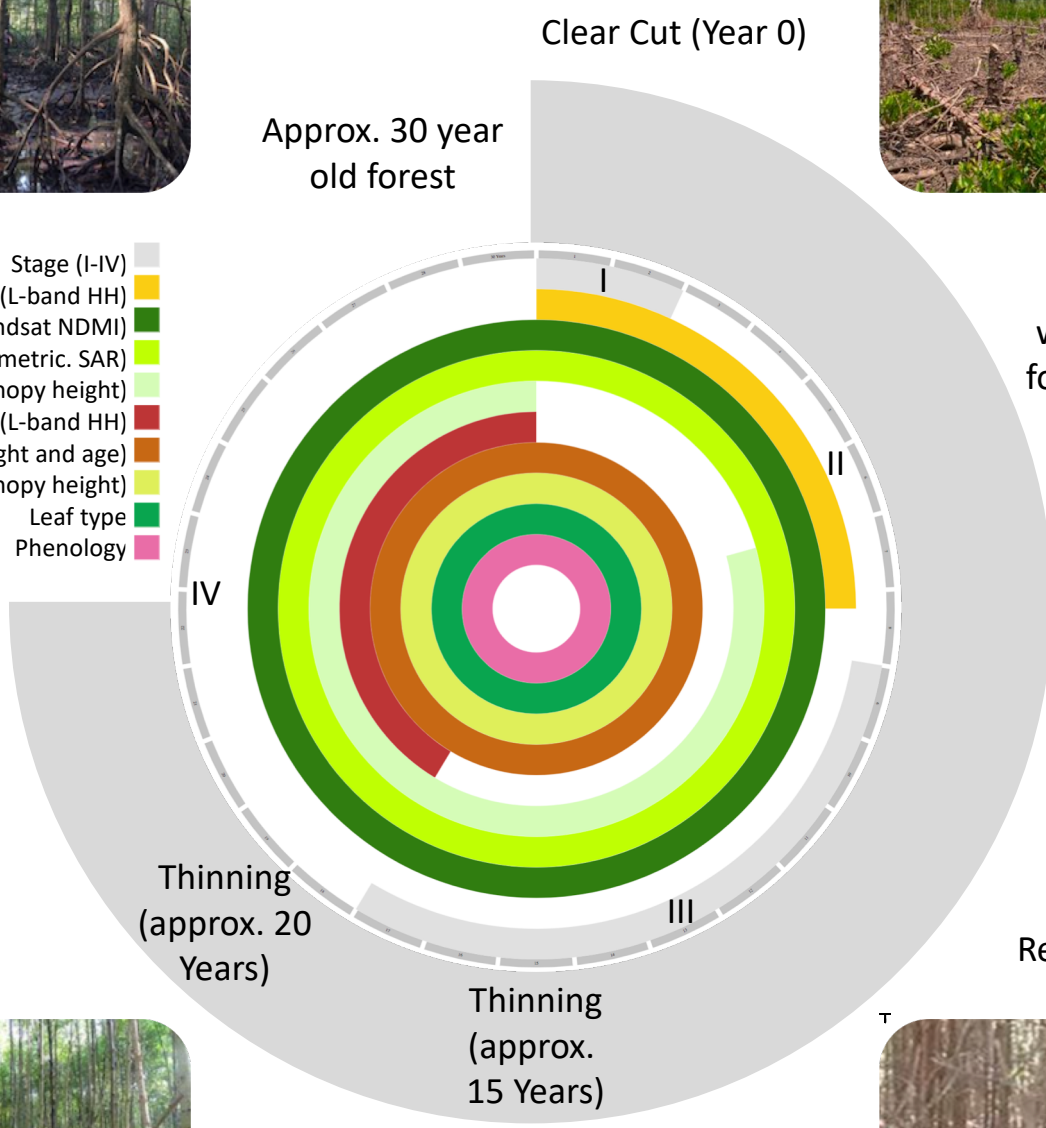
Maturing of *Rhizophora* and progressive formation of larger prop roots

I

II

IV

III

Thinning (approx. 20 Years)

Thinning (approx. 15 Years)

Regrowth